When Ferrocene and Diiron Organometallics Meet: Triiron Vinyliminium Complexes Exhibit Strong Cytotoxicity and Cancer Cell Selectivity

Silvia Schoch, Simona Braccini, Lorenzo Biancalana, Alessandro Pratesi, Tiziana Funaioli, Stefano Zacchini, Guido Pampaloni, Federica Chiellini, Fabio Marchetti

Robust and versatile cationic triiron complexes, obtained from the assembly of ferrocenyl with a di-organoiron structure, display an outstanding cytotoxicity profile which may be related to redox processes provided by the two metallic compartments.

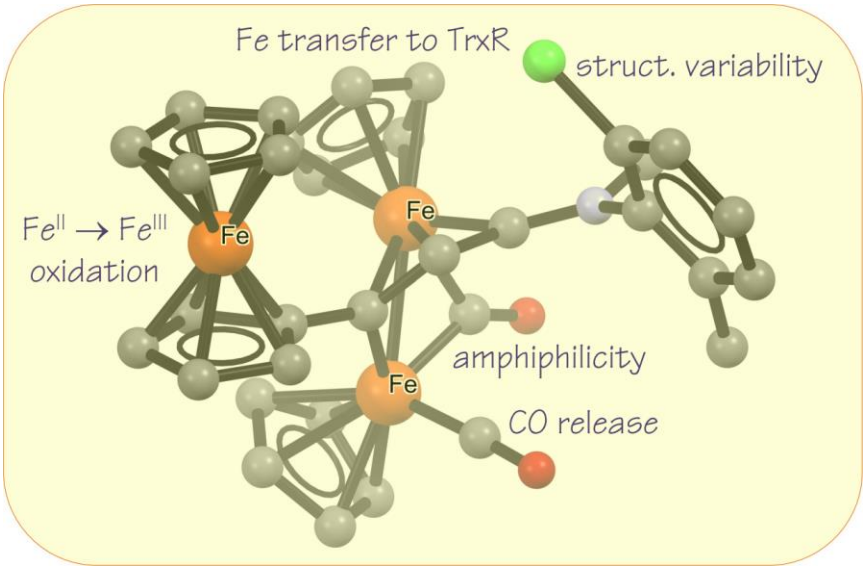

When Ferrocene and Diiron Organometallics Meet: Triiron Vinyliminium Complexes Exhibit Strong Cytotoxicity and Cancer Cell Selectivity

Silvia Schoch,[a] Simona Braccini,[a] Lorenzo Biancalana,[a] Alessandro Pratesi,[a] Tiziana Funaioli,[a] Stefano Zacchini,[b] Guido Pampaloni,[a] Federica Chiellini,[a,*] and Fabio Marchetti [a,*]

[a] University of Pisa, Department of Chemistry and Industrial Chemistry, Via G. Moruzzi 13, I-56124 Pisa, Italy.

[b] University of Bologna, Department of Industrial Chemistry "Toso Montanari", Viale Risorgimento 4, I-40136 Bologna, Italy.

This publication is dedicated to our co-worker and friend Professor Federica Chiellini, who prematurely deceased on 7th March 2021

***Corresponding Author**

To whom correspondence should be addressed: fabio.marchetti1974@unipi.it

Webpage: https://people.unipi.it/fabio_marchetti1974/

Abstract

Cationic triiron complexes resulting from the conjugation of the ferrocenyl skeleton (Fc) with a diiron bis-cyclopentadienyl core through a variable vinyiliminium linker, [$Fe_2Cp_2(CO)(\mu\text{-}CO)\{\mu\text{-}\eta^1\text{:}\eta^3$-

C(Fc)CHCN(R)(R')}]CF_3SO_3 (**[2a-i]CF_3SO_3**, Cp = η^5-C_5H_5, R, R' = alkyl, aryl), were synthesised in 70-94% yields, and also the homologous nitrate salt was prepared in one case (**[2h]NO_3**). The neutral derivatives [$Fe_2Cp_2(CO)(\mu\text{-}CO)\{\mu\text{-}\eta^1\text{:}\eta^3\text{-}C(Fc)CHC(CN)NMe_2\}$], **3**, and [FeCp(CO){CN(Me)(Xyl)CHC(Fc)C(=O)}], **4** (Xyl = 2,6-$C_6H_3Me_2$), were obtained in ca. 70% yields by reactions of the respective precursors **[2h]CF_3SO_3** and **[2i]CF_3SO_3** with NBu_4CN and pyrrolidine, respectively. All products were purified by alumina chromatography and fully characterised by analytical and spectroscopic methods, and by single crystal X-ray diffraction in the cases of **[2a]CF_3SO_3** and **3**. The cytotoxicity of the complexes was assessed on A2780, A2780cisR and BxPC-3 cancer cell lines, and the nontumoral one Balb/3T3 clone A31. Most of the cationic complexes display IC_{50} values in the low micromolar/nanomolar range concerning the cancer cell lines, and up to 35 times higher values on the nontumoral cells. In order to shed light on the mode of action, selected complexes were further characterised by cyclic voltammetry and spectroelectrochemical experiments, and assessed for their potential to trigger ROS production and to interact with a range of biomolecules, i.e. a synthetic dodecapeptide as a simplified model for thioredoxin reductase (**TrxR-pept**), some model proteins (cytochrome c, hen egg-white lysozyme, ubiquitin, bovine serum albumin, superoxide dismutase and human carbonic anhydrase) and one single-strand oligonucleotide (ODN2).

Keywords: Bioorganometallic Chemistry; Metals in Medicine; Ferrocenes; Diiron Complexes; Vinyliminium; Cytotoxicity; Mass Spectrometry.

Introduction

Cancer is a major health issue worldwide, and the development of innovative and effective drugs is an ultimate demand for research.[1] After the revolutionary discovery of the cytotoxic properties of

cisplatin, few platinum(II) compounds have entered clinical treatments but, despite their undoubtful efficacy, they present some significant limitations.[2] In particular, severe side effects are often encountered being associated with the toxicity of platinum, moreover the resistance acquired by tumours over time is problematic.[3] With the aim of overcoming such limitations, platinum(IV) complexes[4] and many others based on different transition metals have been intensively investigated.[5,6] Iron compounds have aroused a great interest in this setting, on account of their relatively low toxicity and the redox chemistry, related to the metal centre, exportable to physiological media.[7] In particular, ferrocenes have been deeply studied for their promising anticancer potential: an appropriate modification of either one or two cyclopentadienyl rings is key to provide a strong activity, which is mostly associated with Fe^{II} to Fe^{III} oxidation, leading to alteration of the cellular redox balance and subsequent production of toxic substances (reactive oxygen species, ROS).[8] Ferrocifens (structure **I** in Figure 1), obtained by tethering the clinical drug tamoxifen to the ferrocene, have emerged since 1996 as the most celebrated category,[9] however they should be carefully formulated for *in vivo* applications due to insufficient water solubility.[8c,10] Then, a diversity of ferrocene-appended pharmacophores has been reported, highlighting a general increase of the anticancer performance with respect to the corresponding organic drugs.[11,12] This approach has been extended to the conjugation of the ferrocene skeleton with suitable metal structures, to exploit synergic effects arising from different metal centres, and examples include Fe-Pt,[13] Fe-Ru,[14] and other hybrid systems.[15] In addition, it was demonstrated that the coupling of two ferrocenyl units by means of short rigid linkers, allowing electronic communication between the two metal atoms, is a feasible strategy to enhance ROS production and cytotoxic activity.[16] Besides ferrocenes, several half-sandwich iron(II) cyclopentadienyl complexes (structure **II** in Figure 1) have attracted attention, since they ensure some variability of the metal coordination set, thus modulating the antiproliferative activity, and offer the opportunity for introducing bioactive ligands with a possible co-adjuvant effect (e.g., carbon monoxide).[17] In general,

this kind of monoiron complexes is conveniently synthesised by oxidative cleavage of the commercial iron(I) dimer [$Fe_2Cp_2(CO)_4$],[18] however the anticancer properties of derivatives of the latter maintaining the dinuclear structure have been almost ignored up to 2019.[19] There are concrete reasons that strongly encourage the advance of this research. In general, a bimetallic core bearing two contiguous metal centres makes available more coordination sites and provides cooperative effects to the bridging sites, enabling reactivity patterns otherwise not feasible on monometallic species.[20] This approach has been largely investigated on diiron complexes in the catalysis field, pointing to the goal of mimicking the active site of [FeFe] hydrogenases.[21] In the medicinal context, it is relevant that a great number of organometallic structures is accessible from [$Fe_2Cp_2(CO)_4$], stabilised by multisite ligand coordination and the co-presence of Cp (π-donor) and CO (π-acceptor) co-ligands, thus allowing to optimise physico-chemical properties for biological purposes.

The availability of up to two coordination sites by sequential displacement of carbonyl ligands is required for the construction of bridging hydrocarbyl fragments from the assembly of small molecular pieces.[22] This procedure leads to cationic [Fe^IFe^I] complexes comprising either an aminocarbyne [23] or a vinyliminium [24] as bridging ligand (structures **III** and **IV** in Figure 1); these complexes are amphiphilic and appreciably water-soluble, and exhibit an antiproliferative activity against cancer cell lines which depends on the ligand substituents. Some complexes of type **III** maintain an excellent cytotoxicity profile even on 3D models.[23] Complexes of type **IV** permit a vast choice of substituents,[25] including the incorporation of bioactive groups regulating the cytotoxic activity.[26] Different mechanisms, mainly ROS production but also protein interaction and weak DNA binding, may contribute to the mode of action of **III** and **IV**.

Here, for the first time, the synergic conjugation of the ferrocenyl moiety with a diiron framework is presented as a strategy to obtain robust mixed-valent triiron compounds featured by a potent cytotoxicity and excellent selectivity towards cancer cell lines.

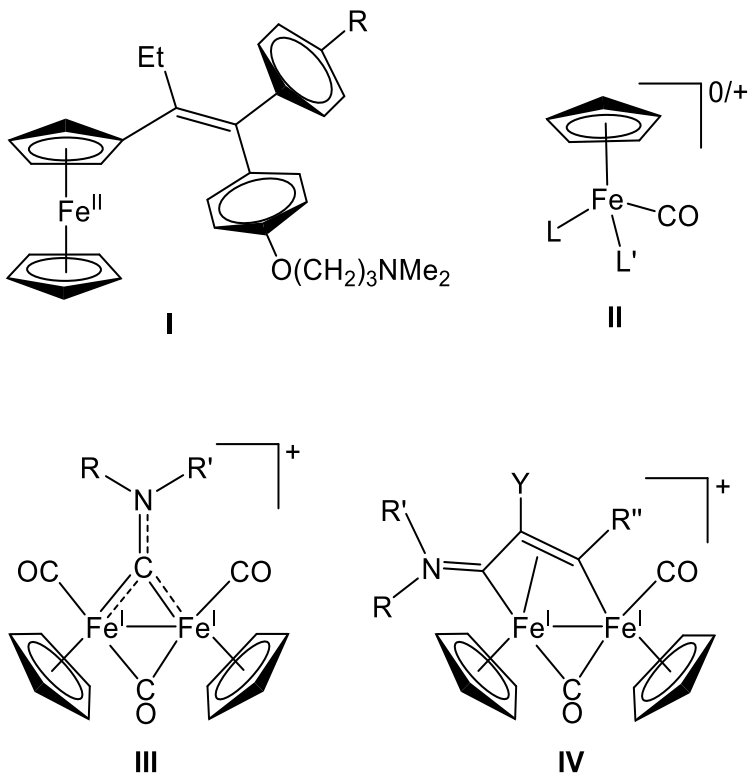

Figure 1. Mono- and diiron cyclopentadienyl compounds with cytotoxic activity: **I**) ferrocifens (Fe^{II}; R = H, OH); **II**) half-sandwich iron complexes (Fe^{II}; L, L' = halide, pseudohalide, carbonyl, (di)phosphine, nitrile, imidazole); **III**) diiron μ-aminocarbyne complexes ($Fe^{I}Fe^{I}$; R, R' = alkyl or aryl; triflate salts); **IV**) diiron μ-vinyliminium complexes ($Fe^{I}Fe^{I}$; R, R' = alkyl or aryl; R'' = alkyl, aryl, carboxylate, $SiMe_3$, thiophenyl, pyridine; Y = H, alkyl, Ph, S/Se group; triflate salts).

Results and discussion

1) Synthesis and characterisation of complexes

Diiron μ-aminocarbyne complexes **[1a-i]CF_3SO_3** were prepared in multigram scales following the published procedures.[23,27] Then, decarbonylation of **[1a-i]CF_3SO_3** was performed with Me_3NO in acetonitrile solution, leading to the known intermediates **[1'a-i]CF_3SO_3**.[25,28] The latter complexes contain a labile NCMe ligand, and the subsequent treatment with ethynylferrocene, in dichloromethane, resulted in the insertion of the alkyne into iron-carbyne bond, upon acetonitrile displacement (Scheme 1). The triiron products, [**2a-i**]**CF_3SO_3**, were purified by alumina chromatography and finally isolated as indefinitely air-stable solids (70-94% yields vs. **[1a-i]CF_3SO_3**). Compounds **[2a-g]CF_3SO_3** are

unprecedented and synthesised without the need of inert atmosphere, thus this convenient procedure was extended to the preparation of the previously reported **[2h-i]CF_3SO_3**.[29] The nitrate salt **[2h]NO_3** is also novel and was prepared from **[1h]NO_3**.[30]

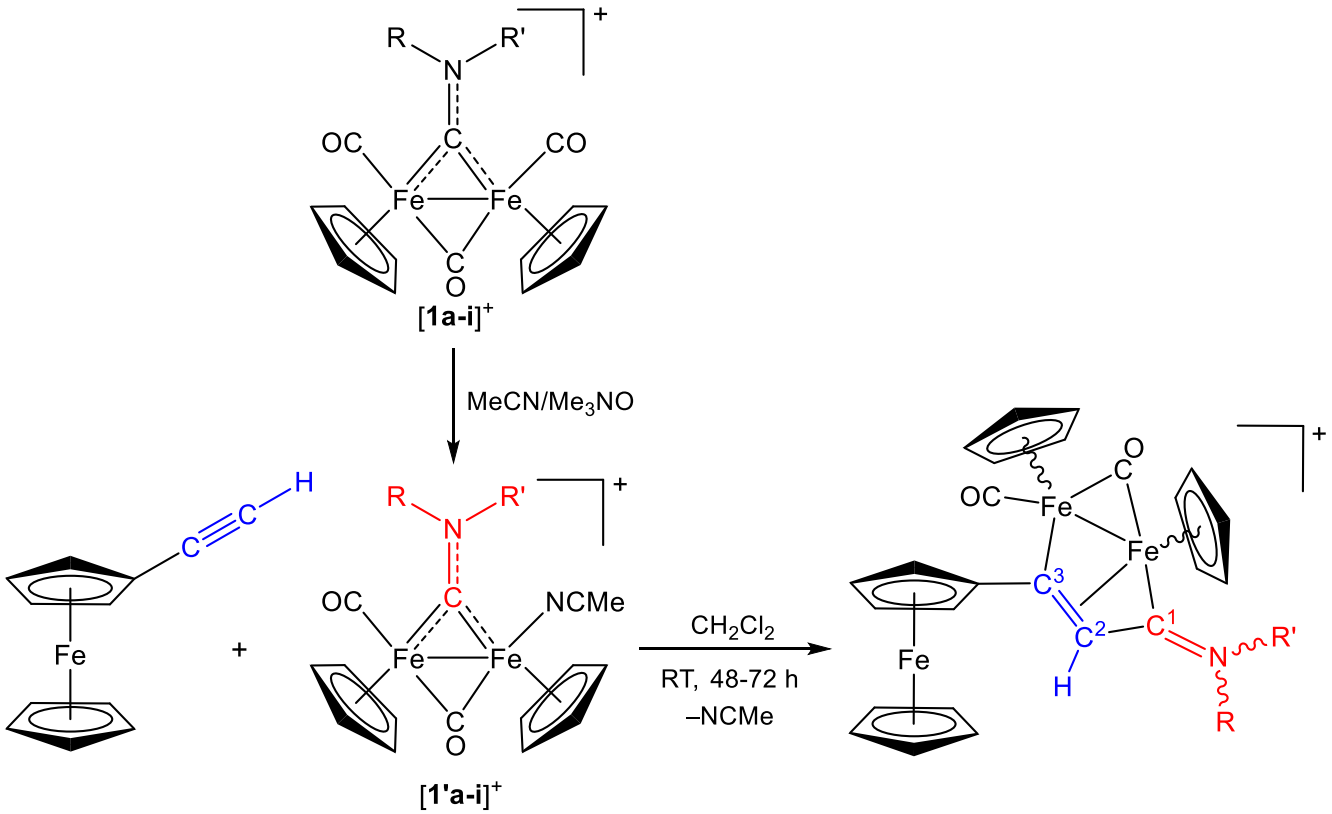

	R	*R'*
[**2a**]$^+$	2,6-C_6H_3(Me)(Cl)	Me
[**2b**]$^+$	4-C_6H_4OMe	Me
[**2c**]$^+$	2-naphthyl	Me
[**2d**]$^+$	CH_2Ph	Me
[**2e**]$^+$	Cy	Me
[**2f**]$^+$	$CH_2CH{=}CH_2$	Me
[**2g**]$^+$	CH_2Ph	CH_2Ph
[**2h**]$^+$	Me	Me
[**2i**]$^+$	Xyl	Me

Scheme 1. Synthesis of ferrocenes with a tethered cationic di-organoiron structure. Cy = C_6H_{11}, Xyl = 2,6-$C_6H_3Me_2$; $CF_3SO_3^-$ as counter anion, [**1h**]$^+$/[**1'h**]$^+$/[**2h**]$^+$ were prepared also as NO_3^- salts.

Products were fully characterised by elemental analysis, high-resolution mass spectrometry, IR (Figures S1-S13) and multinuclear NMR spectroscopy (Figures S14-S38). Note that [Fe^IFe^I]

compounds are diamagnetic due to coupling between the two iron centres. The IR spectra (CH_2Cl_2 solution) share a common pattern, and the most intense absorptions fall within the intervals 1986-2000 cm^{-1} and 1805-1818 cm^{-1}, being related to the terminal and bridging carbonyl ligands, respectively. The absorption ascribable to the iminium C=N bond is sensitive to the nature of the nitrogen substituents, and ranges in between 1621 (**[2a]CF_3SO_3**) and 1692 (**[2h]NO_3**) cm^{-1}. The nitrate anion of **[2h]NO_3** manifests itself with an intense and broad infrared band at 1338 cm^{-1} (spectrum in the solid state).

A careful comparison of the NMR data of the products with the library of data available in the literature for other Fe_2-μ-vinyliminium compounds [24,25,28b] points out the occurrence in solution (acetone-d_6) of *cis*-*trans* isomerism (with reference to the Cp ligands bound to Fe-Fe) and *E*-*Z* isomerism (with reference to the N substituents, when R ≠ R'), *cis*-*E* being generally the most abundant species. *Trans* isomers, when observed, display one Cp resonance which is usually 0.5-0.6 ppm shifted to lower frequency with respect to the corresponding *cis* forms. More in detail, complexes [**2g-h**]$^+$ display only *cis*/*trans* isomerism, due to the identical substituents on the iminium (R = R'), with predominance of the *cis* isomer. For instance, the *cis*/*trans* ratio for [**2g**]$^+$ in acetone-d_6 solution is 6.5, and the stereochemistry of the major isomer was confirmed by ^{1}H NOESY experiments with selective irradiation of both Fe(I)-bound cyclopentadienyls (Figure S39).

On the other hand, *E* and *Z* isomers of [**2a-f**]$^+$ and [**2i**]$^+$ are easily distinguishable based on the resonance related to the N-methyl, inter alia: in the former isomer, such resonance typically falls at higher ^{1}H chemical shift but lower ^{13}C NMR chemical shift [e.g., N-Me in the case of [**2d**]$^+$: δ(^{1}H) = 4.01 ppm (E) and 3.20 ppm (Z); δ(^{13}C) = 42.9 ppm (E) and 47.6 ppm (Z)]. ^{1}H NOESY experiments were carried out for the two major isomers of [**2e**]CF_3SO_3, as a representative example (Figures S40-S41): selective irradiation of the Cp bound to the {Fe(CO)} group corroborated their *cis* stereochemistry whereas the N-methyl resonance was instrumental in assigning the *E* / *Z* configuration. More precisely, upon irradiation of the latter, a NOE effect with the C^{2}H is diagnostic of *Z*

stereochemistry (FeCp and Cy groups on the same side of the C=N double bond); whereas a NOE effect with the cyclopentadienyl indicates *E* stereochemistry. Careful chromatographic operations allowed to isolate small amounts of **[2e]CF_3SO_3** and **[2f]CF_3SO_3** as *cis*/*trans* mixtures of pure *Z*-isomers (vide infra).

The *cis*-*E* isomer was the only one recognised for **[2a]CF_3SO_3** and **[2i]CF_3SO_3**, presumably as a consequence of the bulkiness of the 2,6-disubstituted aryl (R'), pointing away from the {Fe_2Cp_2} platform; however, **[2a]CF_3SO_3** exists as two conformers corresponding to two different spatial arrangements of the Me and Cl aryl substituents, analogously to what previously observed in **[1a]CF_3SO_3**.[31] In every case, the isomer ratios did not change upon prolonged heating of the complexes in THF or methanol at reflux.

Salient $^{13}C\{^1H\}$ NMR features are given by the resonances of the carbons constituting the vinyliminium chain, occurring in the ranges 223.5 – 234.9 ppm (C^1), 50.3 – 56.3 ppm (C^2) and 199.4 – 206.4 ppm (C^3); C^1 and C^3 exhibit a marked (amino)alkylidene and alkylidene nature, respectively (C atom numbering in Scheme 1). The nitrate anion resonates as a sharp singlet at -1.5 ppm in the ^{14}N NMR spectrum of **[2h]NO_3**.

The structure of **[2a]CF_3SO_3** was ascertained by single crystal X-ray diffraction, and two alternative views of the cation are drawn in Figure 2. The cation [**2a**]$^+$ may be alternatively described as a mono-substituted ferrocene connected to the {*cis*-$Fe_2Cp_2(CO)_2$} moiety via a vinyliminium linker showing E-configuration of nitrogen substituents (Figure 2A), or a ferrocenyl-decorated diiron vinyliminium complex (Figure 2B). The C(1)-N(1) distance [1.303(4) Å] supports an iminium character, while the Fe(2)-C(1) distance [1.829(3) Å] is indicative of aminoalkylidene nature, in accordance with the NMR features (Table 1).

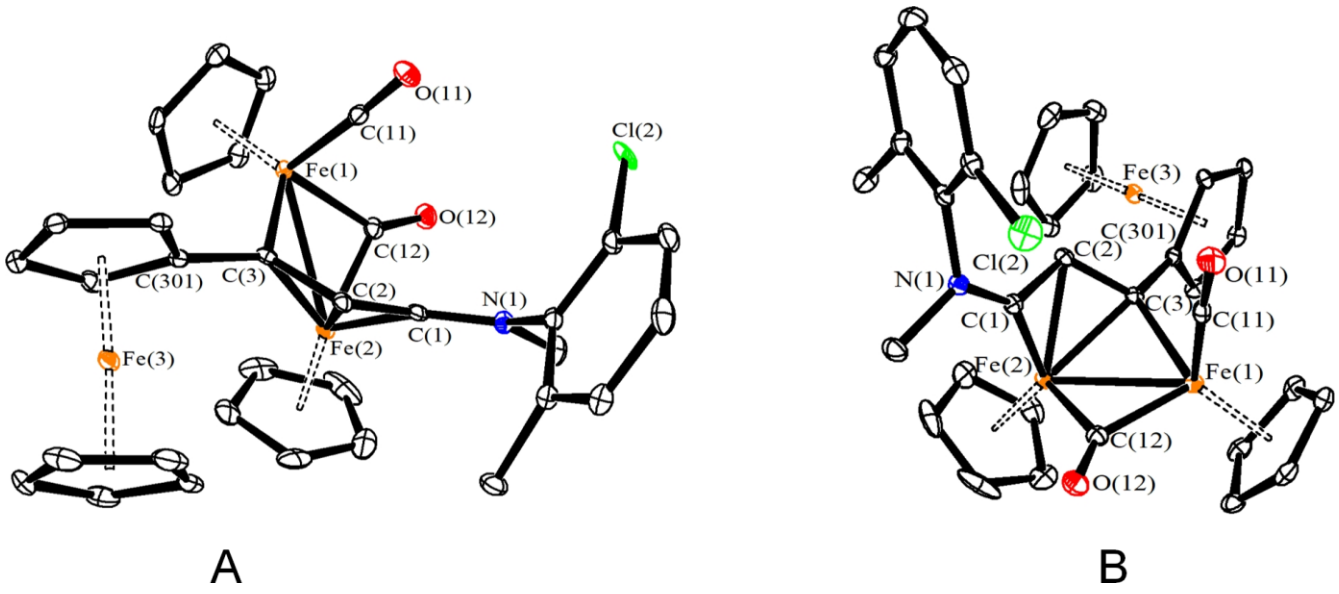

Figure 2. Alternative views of the molecular structure of [**2a**]$^{+}$: A) ferrocene connected to a diiron scaffold via a vinyliminium linker; B) diiron μ-vinyliminium complex decorated with a ferrocenyl. Displacement ellipsoids are at the 30% probability level. H atoms have been omitted for clarity.

On account of the documented chemistry of non-ferrocenyl diiron vinyliminium complexes,[32] we synthesised the neutral derivatives **3** and **4** (Scheme 2). Thus, the reaction of **[2h]CF$_3$SO$_3$** with tetrabutylammonium cyanide, in dichloromethane solution, led to the isolation, after work-up, of the novel [Fe^{I}Fe^{I}Fe^{II}] complex **3** in 70% yield. On the other hand, the previously reported [Fe^{II}Fe^{II}] complex **4**[29,27] was synthesised here by an optimised procedure, consisting in the fragmentation reaction of **[2i]CF$_3$SO$_3$** with pyrrolidine in tetrahydrofuran.

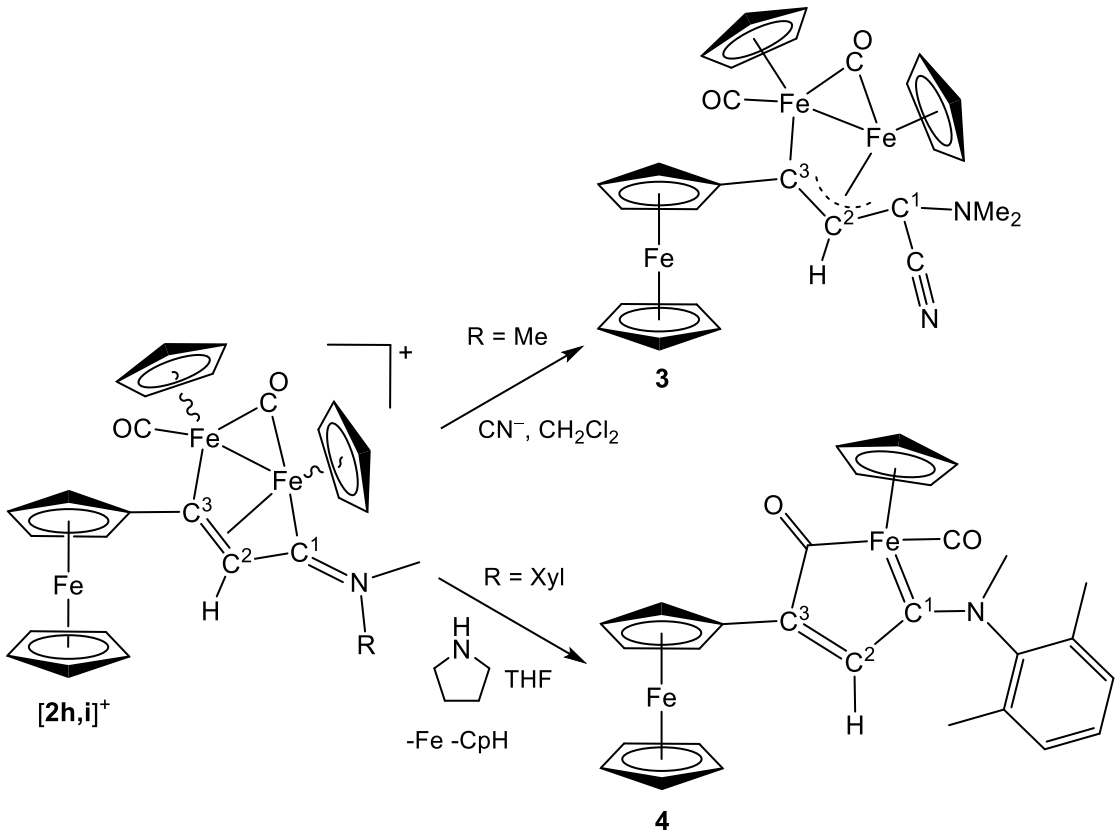

Scheme 2. Synthesis of ferrocenes functionalised with a neutral di- or monoiron structure (Xyl = 2,6-$C_6H_3Me_2$).

The cyanide addition to [**2h**]$^+$ is evident from IR (medium intensity band at 2188 cm^{-1}) and $^{13}C\{^1H\}$ NMR spectroscopy (resonance at 120 ppm) and takes place in a regio- and stereospecific fashion, in analogy to previous findings.[33] The triiron product **3** exists in solution as a single isomeric form with the Fe-Fe cyclopentadienyl rings adopting *cis* geometry (according to NMR). The structure of **3** was confirmed by single crystal X-ray diffraction (Figure 3 and Table 1): it consists of a ferrocene linked to $\{Fe_2Cp_2(CO)_2\}$ through a functionalised allylidene bridge (Figure 3A), which displays a mutual *syn* orientation of the C^2-bound hydrogen and the cyano group. On the other hand, **3** may be viewed as a diiron allylidene complex with a ferrocenyl as allylidene substituent (Figure 3B).

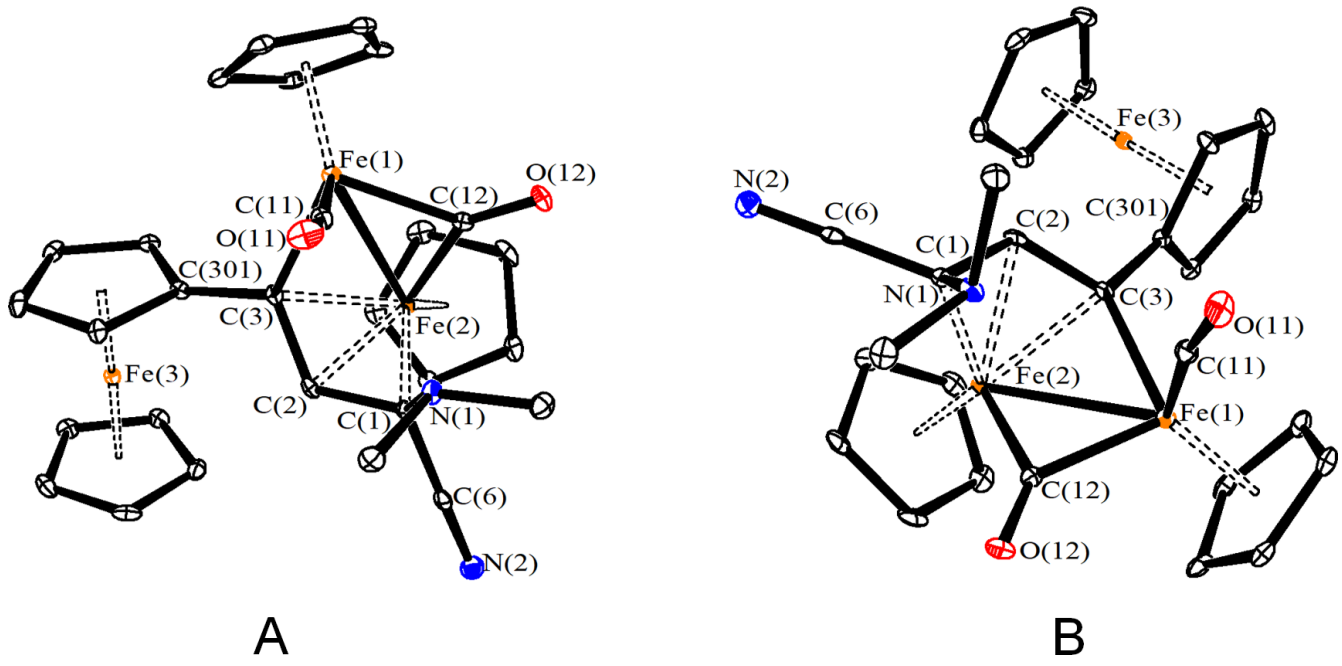

Figure 3. Alternative views of the molecular structure of **3**: A) ferrocene connected to a diiron scaffold via cyano-allylidene linker; B) diiron μ-(cyano)allylidene complex decorated with a ferrocenyl. Displacement ellipsoids are at the 30% probability level. H atoms have been omitted for clarity.

Table 1. Selected bond lengths (Å) and angles (°) for [**2a**]$^+$ and **3**. *Cp_{Ct} is the centroid of the Cp ligand. For Fe(3), Cp^a is the substituted Cp, Cp^b the unsubstituted Cp.

	[**2a**]$^+$	**3**
Fe(1)-Fe(2)	2.5574(7)	2.5379(6)
Fe(2)-C(1)	1.829(3)	2.071(3)
Fe(2)-C(2)	2.073(3)	2.025(3)
Fe(2)-C(3)	2.045(3)	2.025(3)
Fe(1)-C(3)	1.977(3)	1.964(3)
Fe(1)-C(11)	1.759(3)	1.771(3)
Fe(1)-C(12)	1.901(4)	1.922(3)
Fe(2)-C(12)	1.974(4)	1.911(3)
Fe(1)-Cp_{Ct}*	1.743(5)	1.747(5)
Fe(2)-Cp_{Ct}*	1.736(5)	1.716(5)
Fe(3)-Cp^a_{Ct}*	1.645(5)	1.651(5)
Fe(3)-Cp^b_{Ct}*	1.656(5)	1.653(5)
C(11)-O(11)	1.145(4)	1.142(4)
C(12)-O(12)	1.160(4)	1.178(4)
C(1)-N(1)	1.303(4)	1.447(4)

C(1)-C(2)	1.424(5)	1.446(4)
C(2)-C(3)	1.420(5)	1.414(4)
C(3)-C(301)	1.468(5)	1.475(4)
C(1)-C(6)	-	1.467(5)
C(6)-N(2)	-	1.145(4)
Fe(1)-C(11)-O(11)	177.0(3)	169.1(3)
Fe(1)-C(12)-Fe(2)	82.58(15)	82.94(13)
Fe(1)-C(3)-Fe(2)	78.93(12)	79.01(11)
Fe(1)-C(3)-C(2)	120.7(2)	125.0(2)
C(3)-C(2)-C(1)	117.3(3)	123.6(3)
C(2)-C(1)-N(1)	134.2(3)	121.2(3)
Sum at N(1)	359.2(5)	334.4(5)
C(1)-C(6)-N(2)	-	179.3(4)

2) Solubility, inertness and CO release in aqueous solutions

With a view to the biological studies, we preliminarily performed a detailed study on the behaviour of the complexes in aqueous media: these data are compiled in Table 2. The solubility was assessed in D_2O by ^1H NMR and resulted appreciable for those compounds without a N-aryl group. Among triflate salts, **[2h]CF_3SO_3** exhibits the highest water solubility, which is increased by one magnitude order with triflate/nitrate substitution; notably, the solubility of **[2h]NO_3** (approximately 5.5 $g \cdot L^{-1}$) is higher than that estimated for cisplatin (3 $g \cdot L^{-1}$).[34]

The octanol-water partition coefficients (Log P_{ow}) were measured by UV-Vis spectroscopy. Log P_{ow} related to the triflate salts fall within the range 0.26 to 1.48, indicating some amphiphilic character, while that of the nitrate compound **[2h]NO_3** measures -0.48. The neutral complexes **3** and **4** are significantly more lipophilic (Log $P_{ow} \geq 1.5$).

In order to evaluate the robustness in an aqueous environment, first we assessed the residual amount of all complexes after 72 h in D_2O/CD_3OD solution at 37 °C, by means of ^1H NMR spectroscopy using dimethylsulfone (Me_2SO_2) as internal standard (Table 2); ^1H NMR spectra related to **[2a-i]$^+$** were

sufficiently resolved (see for instance Figure S42) to argue for negligible contamination from paramagnetic species, and did not contain signals ascribable to newly formed {Fe-Cp} compounds. Then, analogous NMR experiments were conducted on the ionic complexes in D_2O/DMSO-d_6 solution. In general, the latter complexes are fairly to very robust, and in most cases approximately 70-90% of the initial species was found unaltered after 72 h. Remarkably, a similar behaviour was recognised in the corresponding solutions with the cell culture medium (deuterated DMEM).[35] However, the nature of the iminium substituents appears influencing, and those complexes with two alkyl substituents ([**2e**]$^+$, [**2f**]$^+$, [**2h**]$^+$) show the highest inertness. The naphthyl group induces on **[2c]CF_3SO_3** a drop of stability in the presence of dimethylsulfoxide, possibly related to the coordination ability of this solvent, and this behaviour is confirmed in the cell culture medium.

Neutral complexes **3** and **4** exhibited extensive degradation in aqueous media after 72 hours, affording complicated mixtures of organometallic products which could not be identified.

The slow, partial degradation of triiron complexes is accompanied by the precipitation from the solutions of a small amount of a dark-brown solid. IR and elemental analyses on such solid samples ruled out the presence of organic species, thus suggesting the formation of iron oxides, consistently with previous results on related complexes based on the $\{Fe_2Cp_2(CO)_x\}$ core (x = 2 or 3).[23,24a]

To check the release of carbon monoxide, we performed headspace GC analyses on methanol/water solutions of the complexes stored at 37 °C for 24 h. The released CO corresponds to 0.1 − 0.3 equivalents per mole of triiron complex and might play some adjuvant role in the antiproliferative activity,[36] but targeted studies will be needed to validate this hypothesis.

Overall, experimental outcomes agree in that the cationic triiron complexes, in aqueous media, undergo a slow and irreversible cleavage of the diiron scaffold, leading to the extrusion of Fe^I ions and CO. We previously demonstrated for diiron aminocarbyne complexes (Figure 1, structure **III**) that the same disassembly is accelerated inside the cells and is associated with the cytotoxicity.[23] Note that the

versatile vinyliminium ligand is susceptible to nucleophilic attack by various functional groups,[32] and the resulting derivatives may undergo fast decomposition in aqueous solutions.[37]

Table 2. Behaviour of functionalised ferrocenes in aqueous solutions (see Experimental for details). Solubility in D_2O (^1H NMR, Me_2SO_2 internal standard) and partition coefficients (Log P_{ow}; UV-Vis) at 21±1 °C. Relative stability in D_2O/CD_3OD and CD_3OD/DMEM-d solutions after 72 h at 37 °C (^1H NMR, Me_2SO_2 internal standard). Equivalents of carbon monoxide released in H_2O/CH_3OH solution after 24 h at 37 °C (GC-TCD).

Compound	Solubility / mol·L^{-1}	Log P_{ow}	Residual complex % in D_2O/CD_3OD [a] [b]	Residual complex % in D_2O/DMSO-d_6 [a] [b]	Residual complex % in DMEM-d/CD_3OD [a] [b]	CO equivalents released in H_2O /CH_3OH [a][c]
[**2a**]CF_3SO_3	< 3·10^{-4} [d]	1.05 ± 0.05	59	57	73	0.08
[**2b**]CF_3SO_3	< 3·10^{-4} [d]	0.55 ± 0.05	49	53	50	0.27
[**2c**]CF_3SO_3	< 3·10^{-4} [d]	0.47 ± 0.02	70	37	≈ 25	0.17 ± 0.09
[**2d**]CF_3SO_3	< 3·10^{-4} [d]	0.66 ± 0.05	77	48 (2:1 v/v)	63	0.18
[**2e**]CF_3SO_3	≈ 3·10^{-4}	0.77 ± 0.06	78	84 (2:1 v/v)	88	0.15
[**2f**]CF_3SO_3	8·10^{-4}	0.49 ± 0.02	90	81 (2:1 v/v)	86	0.14
[**2g**]CF_3SO_3	< 3·10^{-4} [d]	1.48 ± 0.03	75	67 (2:1 v/v)	80	0.15
[**2h**]CF_3SO_3	1.0·10^{-3}	0.26 ± 0.03	83	81 (2:1 v/v)	75	0.13
[**2h**]NO_3	9.8·10^{-3}	-0.48 ± 0.02	89	91 (2:1 v/v)	89	0.14
[**2i**]CF_3SO_3	< 3·10^{-4} [d]	1.05 ± 0.04	72	70	70	0.08
3	< 3·10^{-4} [d]	> 2	0	0	0	[e]
4	< 3·10^{-4} [d]	1.5 ± 0.1	*ca.* 30	*ca.* 20	*ca.* 15	[e]

[a] 1:1 v/v mixtures for ionic compounds unless otherwise stated, 3:1 v/v mixtures for neutral compounds. [b] Calculated by ^1H NMR with respect to the initial spectrum (Me_2SO_2 internal standard). [c] Molar ratio with respect to the starting complex ($eq_{CO} = n_{CO}/n_{complex}$). The amount of carbon monoxide was determined by GC-TCD analysis. Relative standard deviation below 10% except where otherwise noted. [d] Below the lowest value of quantitation. [f] CO release was detected, but a reliable quantitation was not possible due to limited complex solubility.

3) Electrochemistry

The redox chemistry of selected cationic complexes and that of the neutral one **3** was investigated by cyclic voltammetry at a platinum electrode in DMSO/[N^{n}Bu$_4$]PF_6 0.1 M. The formal potentials for the observed electron transfers are compiled in Table 3 and, as an example, the CV performed on **[2e]CF_3SO_3** is shown in Figure 4. The voltammetric profiles of the cationic complexes evidence either one reduction process, appearing as a two-electron one, or two very closely spaced one-electron reduction processes, at potential values within the range −1.16 to −1.37 V (*vs*. $FeCp_2$). In particular, the

value related to **[2h]NO$_3$** is almost identical to that found in the same conditions for the analogous complex [$Fe_2Cp_2(CO)(\mu\text{-}CO)\{\mu\text{-}\eta^1\text{:}\eta^3\text{-}C(Ph)CHCNMe_2\}]CF_3SO_3$, **[2j]CF$_3SO_3$** (see Figure 1, structure **IV**: R = R' = Me, R'' = Ph, Y = H), containing a phenyl in the place of the ferrocenyl moiety.[24a] Thus, the observed reduction(s) are assigned to the [Fe^I-Fe^I] core, and are complicated by subsequent chemical reactions, as indicated by the appearance of new oxidation processes during the back scan toward positive potentials, in the second cycle of the voltammetric experiment (Figure 4, red line).

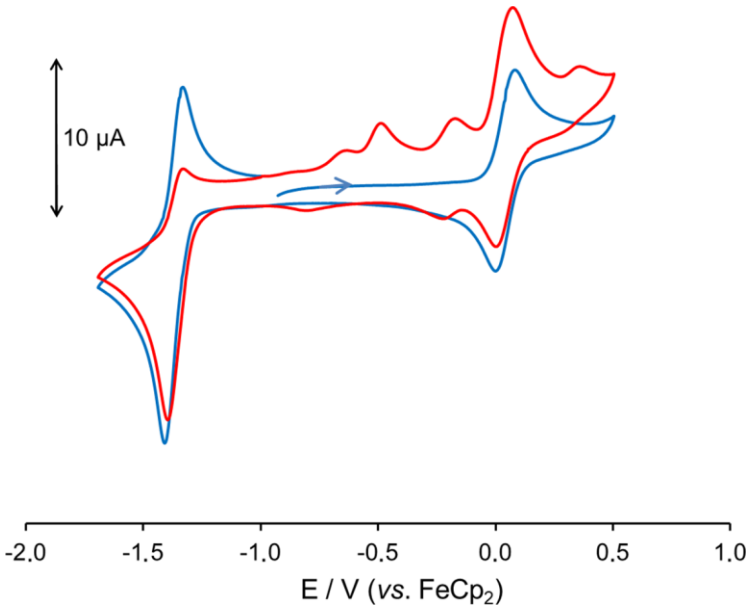

Figure 4. Double cycle voltammetry of **[2e]CF$_3$SO$_3$** recorded at a platinum electrode in 0.1 M [N^nBu_4]PF_6/DMSO solution (blue line, first cycle; red line, second cycle). Scan rate: 0.1 V·s^{-1}.

The cationic complexes **[2a,2e,2f]CF$_3$SO$_3$** and **[2h]NO$_3$** exhibit one electrochemically reversible or quasi-reversible oxidation between +0.04 and +0.09 V (*vs*. $FeCp_2$). Remarkably, these values are lower than the potential measured for ethynylferrocene (+0.17 V), highlighting that the relative tendency for the ferrocenyl Fe^{II} centre to be oxidised is fully preserved in complexes of the type [**2**]$^+$ despite the net cationic charge. Conversely, the non-ferrocenyl diiron complex **[2j]CF$_3$SO$_3$** undergoes oxidation at a significantly higher potential (+0.48 V). Hydrodynamic voltammetry at a rotating-disk electrode verified that, during the reduction, the limiting current is approximately double with respect to that of

the oxidation. These features, combined with the results of the spectroelectrochemical investigation (vide infra), suggest that the one-electron oxidation is almost centred at the ferrocenyl moiety. The chemical reversibility varies with the nitrogen substituent and, for example, the i_c/i_a current ratio measured at 0.1 V s^{-1} is 1 for the electrochemically reversible diffusion-controlled oxidation of **[2e]CF_3SO_3**, whereas it is 0.61 for the electrochemically quasi-reversible process of **[2h]NO_3**. The ferrocenyl-centred oxidation makes the removal of a second electron from [**2**]$^{2+}$ electrostatically unfavourable and, in the examined potential window (up to +0.90 V), no other oxidation process was detected.

With the aim of spectroscopically characterising the oxidised products, we investigated the one-electron removal step from **[2e]CF_3SO_3** by *in situ* IR spectroelectrochemistry in an optically transparent thin-layer electrochemical (OTTLE) cell. When the potential of the working electrode was progressively increased from 0.0 to +0.9 V (*vs.* Ag pseudo-reference electrode), a slight upshift (about 7 cm^{-1}) of the terminal and bridging carbonyl bands of [**2e**]$^+$ was observed (from 1976 and 1798 cm^{-1} to 1983 and 1805 cm^{-1}, respectively), see Figure S43. This fact agrees with the assumption that the reversible one-electron removal mainly regards the ferrocenyl portion of the complex, and therefore does not significantly affect the carbonyl ligands bound to the diiron core. Compared to the CV, the lower stability of the electrogenerated [**2e**]$^{2+}$ was recognised in the time scale of the spectroelectrochemical experiment, since the backward reduction step did not completely restore the initial spectrum (Figure S44).

The water solubility of **[2h]NO_3** revealed adequate to investigate the electrochemical behaviour of this complex also in a phosphate buffer solution (pH 6.7): the reversible oxidation was observed at the formal potential of +0.10 V *vs.* $FeCp_2$ (ΔE = 80 mV at a scan rate of 0.1 V s^{-1}), that is +0.51 V vs SHE. On the other hand, the reduction occurred at the potential of –1.07 V *vs.* $FeCp_2$ (–0.66 V *vs* SHE) and was found irreversible in the aqueous medium.

According to the literature, the biologically relevant redox potentials approximately cover the window −0.4 to +0.8 V [38] *vs* SHE, therefore all the cationic complexes investigated here possess a biologically accessible and reversible oxidation process. Furthermore, their reduction in the tumour environment might be viable too, especially for N-aryl-substituted complexes (Table 3), on considering that, in the cancer cells, the low O_2 content and the presence of an excess of lactic acid decrease the solution pH and determine, particularly at the centre of the tumour, a lower electrochemical potential with respect to the surrounding normal tissues.[39]

The CV profile of **3** in dimethylsulfoxide solution (Figure S45) closely resembles those of homologous diiron complexes without the ferrocenyl unit,[33] and consists of one electrochemically quasi-reversible reduction and one irreversible multi-electronic oxidation, complicated by fast chemical reactions, respectively at −1.92 and −0.01 V. A further oxidation, apparently chemically reversible, was recognised at +0.17 V, presumably centred on the ferrocenyl unit of a derivative originating from the first oxidation.

In summary, cationic triiron complexes [**2a-i**]$^+$ are expected to exhibit the Fe^{II} / Fe^{III} reversible redox couple typical of simple ferrocenyl compounds,[40] which is relevant to the antiproliferative activity;[41] in addition, a reduction might be also viable for some compounds of the series displaying the most favourable potentials.

Table 3. Formal Electrode Potentials (V, *vs* $FeCp_2$) and peak-to-peak separations (mV) for the redox changes exhibited by HC≡CFc, complexes [**2a**,**2e**,**2f**,**2h,2j**]**CF_3SO_3** and **3**, in DMSO/$[N^nBu_4]PF_6$ 0.1 M.

Compound	Oxidation			Reduction			
	$E°'_1$	ΔE_1[a]	$E°'_2$	$E°'_3$	ΔE_3[a]	$E°'_4$	ΔE_4[a]
HC≡CFc	0.14	83					
[2a]CF_3SO_3	0.09	85		−1.16	86	−1.26	60
[2e]CF_3SO_3	0.04	70		−1.37	50		
[2f]CF_3SO_3	0.04	88		−1.30	60		
[2h]NO_3	0.07	90		−1.31	48		

[2h]NO_3[c]	0.10	80		–1.07[b]	
[2j]CF_3SO_3	0.48[b]			–1.30	122
3	0.17	90	–0.01[b]	–1.92	130

[a] Measured at 0.1 V s^{-1}. [b] Peak potential value for irreversible processes. [c] In phosphate buffer solution (pH 6.7) at a glassy carbon electrode. **[2j]CF_3SO_3** = [$Fe_2Cp_2(CO)(\mu\text{-}CO)\{\mu\text{-}\eta^1\text{:}\eta^3\text{-}C(Ph)CHCNMe_2\}$]$CF_3SO_3$.

4) Cytotoxicity

The antiproliferative activity of the iron complexes was assessed on three cancer cell lines (A2780, A2780cisR, BxPC-3) and one nontumoral cell line (Balb/3T3 clone A31). The reference drug cisplatin and ethynylferrocene, HC≡CFc, were used as references. The resulting IC_{50} values, obtained after 72 hours of exposure, are compiled in Table 4. In general, the ionic triiron complexes are strongly cytotoxic against the investigated cancer cell lines, and the IC_{50} related to **[2a]CF_3SO_3** and **[2i]CF_3SO_3** occur in the nanomolar range. Note that these latter compounds combine a Log P_{ow} value around 1 with an appreciable inertness in the biological medium (Table 2). Compounds **[2a-i]CF_3SO_3** exert a comparable activity against cisplatin-sensitive (A2780) and cisplatin-resistant cells (A2780cisR), suggesting that their mode of action overcomes resistance issues. Furthermore, they manifest a clear selectivity for cancer cells compared to the nontumoral line: the estimated selectivity index (S.I., average value referred to the three cancer cell lines) is impressively higher for all the compounds of the series when compared to cisplatin, and reaches the outstanding value of 35 for **[2i]CF_3SO_3**. The cytotoxicity of **[2h]NO_3** was measured against A2780 cells and is comparable to that of **[2h]CF_3SO_3**, indicating that the choice of nitrate as counter anion may provide useful effects in terms of water solubility of the salt without affecting the activity of the cation. Note that IC_{50} results obtained for **Z-[2e]CF_3SO_3** and **Z-[2f]CF_3SO_3** do not substantially differ from those of the corresponding mixtures of E/Z isomers (vide infra): this feature suggests that, although the analysed complexes may exist in solution as mixtures of stereoisomers, these exert similar activities. The neutral complexes **3** and **4** display a markedly reduced selectivity compared to the corresponding ionic parent complexes

[2h]CF_3SO_3 and **[2i]CF_3SO_3**, and **4** is only moderately active against cancer cells despite its lipophilicity (see Table 2). On the other hand, ethynylferrocene was inactive towards the investigated cell lines, evidencing that the ferracyclic motif in **3** and **4** (in the place of the alkynyl unit) induces a cytotoxic effect. The disappointing performance of **3** and **4** is probably correlated with the poor stability of these compounds in aqueous media (see above).

Table 4. IC_{50} values (μM) determined for complexes **[2a-i]CF_3SO_3**, **[2h]NO_3**, **3**, **4**, ethynylferrocene (HC≡CFc) and cisplatin on human ovarian carcinoma (A2780), human ovarian carcinoma cisplatin-resistant (A2780cisR), human pancreatic adenocarcinoma (BxPC-3) and murine embryonic fibroblast (Balb/3T3 clone A31) cell lines after 72 h exposure. Values are given as the mean ± SD. Selectivity index (S.I.) calculated, for each compound, as the average value of the ratio between IC_{50} related to Balb/3T3 and each cancer cell line, respectively.

Compound	A2780	A2780cisR	BxPC-3	Balb/3T3	S.I.
[2a]CF_3SO_3	0.77 ± 0.04	1.17 ± 0.04	5.8 ± 0.4	11 ± 1	9
[2b]CF_3SO_3	3.0 ± 0.6	5.2 ± 0.4	25 ± 2	20 ± 2	4
[2c]CF_3SO_3	3.2 ± 0.5	5.1 ± 0.3	6 ± 4	17 ± 3	4
[2d]CF_3SO_3	2.0 ± 0.5	2.9 ± 0.7	20 ± 4	18.7 ± 1.5	6
[2e]CF_3SO_3	1.8 ± 1.6	2.7 ± 0.7	17 ± 3	19 ± 5	6
Z-[2e]CF_3SO_3	3.4 ± 0.8	4.7 ± 0.4	--	22.7 ± 1.2	6
[2f]CF_3SO_3	3.6 ± 0.2	6.7 ± 0.7	27 ± 3	67 ± 7	10
Z-[2f]CF_3SO_3	6.0 ± 0.4	14 ± 3	--	72 ± 14	9
[2g]CF_3SO_3	1.3 ± 0.1	1.4 ± 0.7	4.3 ± 0.5	8.3 ± 1.4	5
[2h]CF_3SO_3	4.4 ± 0.8	5.1 ± 0.9	> 100	79 ± 1	11
[2h]NO_3	6.1 ± 0.9	--	--	--	
[2i]CF_3SO_3	0.3 ± 0.1	0.23 ± 0.05	10.9 ± 1.2	13.2 ± 0.9	35
3	6.0 ± 0.7	5.9 ± 1.4	33.2 ± 1.4	16 ± 2	2
4	25 ± 2	50.1 ± 0.1	67 ± 5	96 ± 2	2
HC≡CFc	> 100	> 100	--	> 100	--
cisplatin	0.40 ± 0,07	7.2 ± 0.6	4.6 ± 0.4	0.8 ± 0.2	1

To shed light on the mechanism of action, representative complexes were selected for targeted studies that will be discussed in the following.

5) Iron cellular uptake

The triiron complexes **[2a]CF_3SO_3**, **[2f]CF_3SO_3** and **[2h]NO_3** underwent iron uptake experiments on A2780 ovarian cancer and Balb/3T3 clone A31 nontumoral cell lines. Following 24 h incubation, the amount of internalised iron was obtained by ICP-AES, subtracting the level of physiological iron normally present inside the selected cell lines. The results, reported in Table 5, indicate an augmented iron level in all cell cultures treated with the complexes, and highlight the significantly better uptake of **[2a]CF_3SO_3** with respect to **[2f]CF_3SO_3** and **[2h]NO_3**, in alignment with the higher lipophilicity of the former complex (see Table 2). However, the uptake of **[2a]CF_3SO_3** is not dissimilar in A2780 and Balb/3T3 cell lines, suggesting that the strong selectivity displayed by this complex is not consequent to a privileged internalisation within cancer cells rather than nontumoral ones. Interestingly, a similar conclusion was recently traced for promising diiron aminocarbyne drug candidates (Figure 1, structure **III**).[23]

Table 5. Iron uptake in analysed cell lines measured with ICP-AES.

Compound	Fe level (10^{-8} µg/cell)[a]	Corrected Fe level (10^{-8} µg/cell)
Control [b]	3.8 ± 1	--
[2a]CF_3SO_3 [c]	20.0 ± 0.3	16.2 ± 0.3
[2f]CF_3SO_3 [c]	11.2 ± 0.2	7.4 ± 0.2
[2h]NO_3 [c]	10.8 ± 0.5	7.0 ± 0.5
[2a]CF_3SO_3 [d]	18.5 ± 0.3	14.7 ± 0.3

[a] Mean of three different biological replicates; [b] untreated cells; [c] data related to A2780 cells; [d] data related to Balb/3T3 clone A31 cells. The "corrected Fe level" has been calculated by subtraction of the naturally present iron content ("control") from the total iron content in treated cells.

6) ROS production

A selection of complexes was assessed for intracellular production of reactive oxygen species (ROS), which was monitored by fluorescence measurements using the DCFH-DA assay. Thus, A2780 and A2780cisR cells were continuously exposed to **[2a]CF_3SO_3**, **[2d]CF_3SO_3**, **[2e]CF_3SO_3**, **[2f]CF_3SO_3**,

[2i]CF_3SO_3 and **3** (10 μM concentrations). Cisplatin was used as a reference metallodrug, while H_2O_2 and menadione (100 μM) were alternatively used as positive controls; cells incubated with comparable concentration of DMSO in supplemented cell culture medium, in the absence of any additional compound, were used as negative control. In general, a high intracellular ROS level, compared to menadione, was detected after ca. 20 hours of treatment with the triiron complexes, and progressively raised up to 24 hours, without a significant difference between A2780 and A2780cisR cell lines (Figure 5A-B). Among iron complexes, **[2a]CF_3SO_3** emerged for eliciting the highest ROS generation in both cell lines, and only **[2i]CF_3SO_3** induced a lower ROS production than that provided by menadione. With **[2a]CF_3SO_3**, **[2e]CF_3SO_3**, **[2f]CF_3SO_3**, **3** and menadione, a production of ROS statistically different from the negative control ($p < 0.05$) initiated within the first 3 hours (Figures S46-S47).

Different processes may contribute to the observed increased formation of ROS. More in detail, both the oxidation of the ferrocenyl unit and the disassembly of the diiron core are likely to play important roles, with a possible additional contribution arising from complex reduction (vide infra). In fact, while the iron(I) oxidation state in the diiron core is stabilised by the set of ligands, Fe^{I} ions released upon disaggregation of the organometallic structure are expected to readily undergo oxidation once liberated in an aqueous environment. The decay of the ferrocenyl unit (release of Fe^{II} ion) might also be relevant to ROS, in alignment with previous findings.[42] It is reasonable that the intracellular liberation of the iron ions does not lead to iron oxides, in contrast to what is observable in simple aqueous solutions where potential coordinating agents are absent. In this respect, in the following section we will supply evidence for efficient iron ion capture by thioredoxin reductase.

However, the limited ROS production detected in the presence of **[2i]CF_3SO_3**, being the most cytotoxic compound of the series, suggests that the mode of action of the triiron complexes may be not explicated only in terms of ROS generation, and probably involves other mechanisms and/or cellular targets.

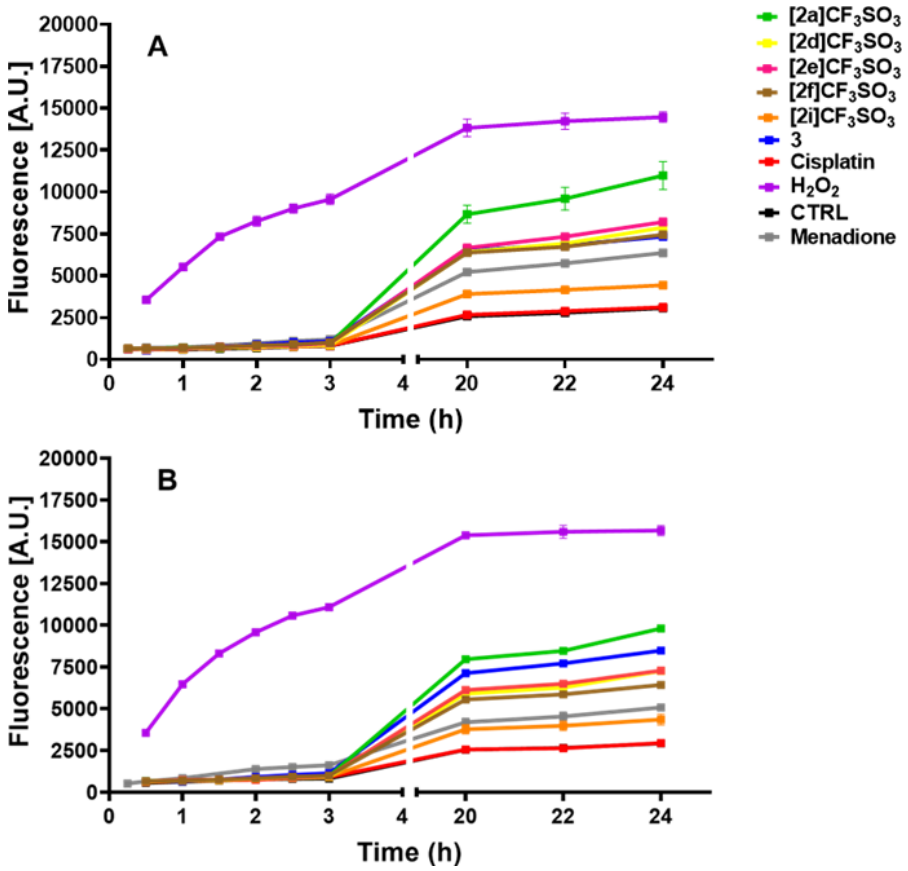

Figure 5. Fluorescence kinetics measurements of intracellular reactive oxygen species (ROS). (**A**) A2780 and (**B**) A2780cisR cells incubated for 24 hours with 10 μM of complexes and 5% atmosphere of CO_2 at 37 °C. H_2O_2 (100 μM) and menadione (100 μM) as positive controls. Analyses were conducted in triplicate and data are represented as mean ± SD.

7) ESI-MS studies on the interaction with biomolecules

Complex **[2a]CF_3SO_3**, featured by strong cytotoxicity and selectivity against all the three cancer cell lines, was challenged also with a panel of different biomolecules. More precisely, three small model proteins,[43] i.e., cytochrome c (Cyt c), hen egg-white lysozyme (HEWL) and ubiquitin (Ub), and three biologically relevant proteins, i.e. bovine serum albumin (BSA), superoxide dismutase (SOD) and human carbonic anhydrase I (hCA I), were considered.[44,45] The protein solutions were individually incubated with **[2a]CF_3SO_3** (at a fixed 3:1 metal to protein molar ratio) for 24 hours at 37 °C. Subsequently, high-resolution ESI mass spectra were recorded for the various samples through direct infusion. As a matter of fact, all spectra showed only the peak corresponding to the unreacted protein,

thus indicating the absence of metalation (Figures S57-S63). This outcome suggests that the action of the complexes may be addressed to specific intracellular targets, whereas off-target reactions with other cellular or plasma proteins are improbable, thus limiting the chance for undesired side effects.

Thioredoxin reductase (TrxR) is an important and ubiquitous flavoenzyme critically involved in the regulation of intracellular redox metabolism, and targeting TrxR has been regarded as a promising strategy for cancer drug development.[46] It has been demonstrated that TrxR inhibition plays an important role in the antiproliferative activity of some iron complexes.[47] We recently disclosed a significant TrxR inhibitory activity of diiron aminocarbyne complexes (Figure 1, structure **III**);[23,48] then, we proved that high-resolution electrospray ionisation mass spectrometry (ESI-Q-TOF) using a model synthetic dodecapeptide (**TrxR-pept**) is fully diagnostic to study the interaction with the complexes.[25] The use of such modelling[49] avoids the direct use of TrxR, being the amount required for mass spectrometric investigation not easily available and extremely expensive. **TrxR-pept** mimics the C-terminal hTrxR(488-499) active site of the TrxR enzyme, corresponding to the amino acidic sequence {Ac-SGGDILQSG[CU]G-NH_2} and the peculiar {-Cys-Sec-} motif (Cys = cysteine; Sec = selenocysteine). By means of the high-resolution electrospray ionisation mass spectrometry (HR-ESI-MS), we ascertained that also a family of diiron vinyliminium complexes hold a potential in inhibiting thioredoxin reductase.[25] Thus, we decided to extend this investigation to the selection of triiron complexes **[2a]CF_3SO_3**, **[2f]CF_3SO_3** and **[2h]NO_3**. Aqueous solutions containing **TrxR-pept** and each metal complex (1:1 molar ratio) were incubated for 24 h at 37 °C, and their mass spectra were subsequently recorded. In the mass spectrum obtained with **[2a]CF_3SO_3** (Figure 6), the main peak at *m/z* 1183.3889 corresponds to the monoprotonated peptide, [**TrxR-pept** + H]$^+$, and the other two signals at *m/z* 1205.3708 and 1221.3437 are related to the peptide adducts with sodium and potassium, respectively ([**TrxR-pept** + M]$^+$). The signal at *m/z* 1237.3108 is attributable to the interaction between **TrxR-pept** and **[2a]CF_3SO_3**, evidencing the formation of a [**TrxR-pept** + Fe – H]$^+$ adduct (Figure

S64). Therefore, TrxR might be a cellular target, as previously ascertained for diiron aminocarbyne complexes (see above), and enzyme inhibition could be effective by transfer of one iron atom released from the activation/disruption of the diiron scaffold inside the cells.

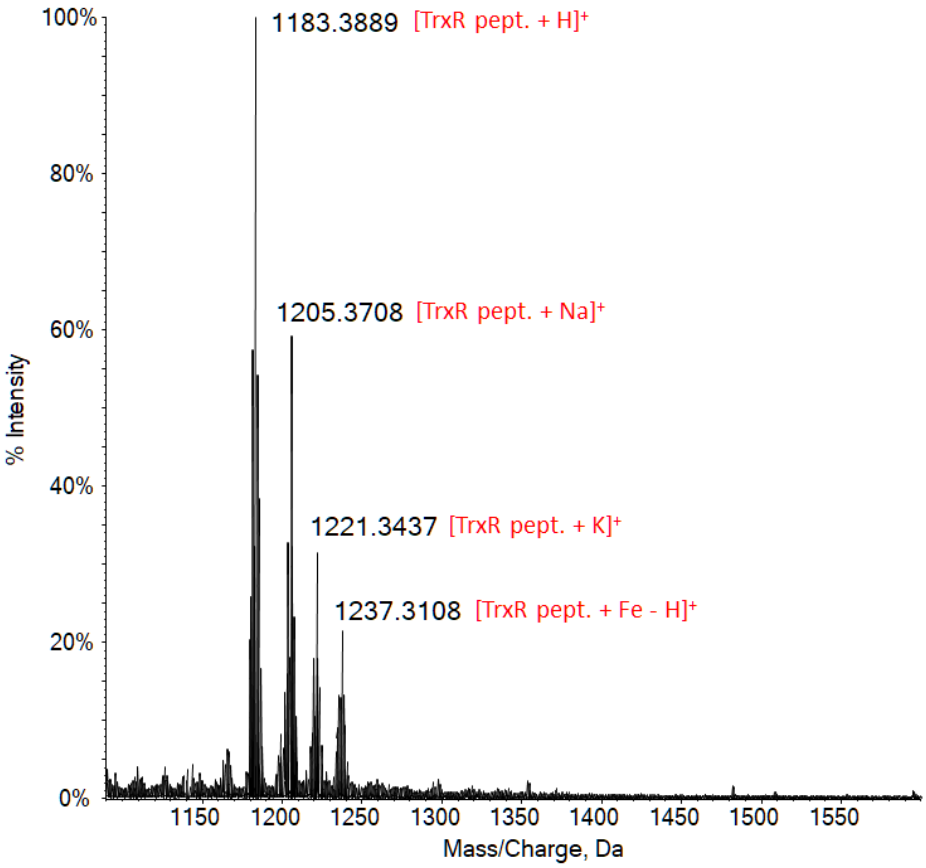

Figure 6. High-resolution ESI mass spectra of $5 \cdot 10^{-6}$ M solution of the model dodecapeptide **TrxR-pept** in water, incubated with [**2a**]CF_3SO_3 for 24 h at 37 °C. 1:1 peptide to complex ratio. 0.1% v/v of formic acid was added just before infusion.

The HR-ESI mass spectra acquired with **[2f]CF_3SO_3** and **[2h]NO_3** resemble that described for **[2a]CF_3SO_3** and are supplied as Supporting Information (Figures S65-S66). As a reference, **TrxR-pept** was allowed to contact with ferrocene; in this case, the formation of [**TrxR-pept** + Fe – H]$^+$ was much slower than in the presence of **[2a,f,h]**$^+$; the targeted adduct was absent in solution after 6 h of incubation, and a modest amount was detected only after 24 h. This experiment outlines that the [Fe^I-Fe^I] core, rather than the ferrocenyl moiety, may behave as prevalent source of iron for thioredoxin

reductase. Although we have been not able to unambiguously clarify the iron-binding site, we can infer that the coordination mode suitable to match the correct mass and charge, furnished by HR-ESI-MS analysis, involves the deprotonated aspartic acid residue, the cysteine thiol group and the selenocysteine selenol group within **TrxR-pept**. Probably, the reductive power of Fe^{I} is crucial to assure a fast reaction with the peptidic {-S-Se-} bridge.

To outline the binding properties with a simplified model for the genomic target,[50] **[2a]CF_3SO_3** was incubated with a small, single-strand GG-rich oligonucleotide (ODN2; 5'-CTACGGTTTCAC-3'); subsequent ESI-MS analysis did not reveal any adduct formation. This data is in alinement with previous findings on related diiron vinyliminium complexes lacking the ferrocenyl unit, for which the absence of a potential DNA binding was ascertained.[24a]

Conclusions

A family of easily available and robust ferrocenes, derivatised with a vinyliminium moiety as a linker to a diiron core, has been synthesised and investigated for the anticancer potential. Cationic triiron complexes synergistically combine the redox behaviour of the ferrocenyl moiety with the amphiphilicity and the versatility of the diiron vinyliminium structure, resulting in an advantageous cytotoxicity profile. Stability data, Log P_{ow} values, iron cellular uptake, and targeted biological studies indicate that **[2a-i]CF_3SO_3** may enter into the cells, where they exert their antiproliferative activity, bypassing degradation pathways upon interaction with common proteins. The uncommon dual electrochemical behaviour shown by the complexes (both oxidation and reduction appear viable) and the extensive disassembly of the organometallic structure are probably fundamental features favouring the imbalance of the cell redox system. Presumably, the decay of the diiron core is accelerated intracellularly, and thioredoxin reductase could play a role in this regard by abstracting one iron ion, thus providing at the same time a chance for the inhibition of this key enzyme. Intriguingly, the

outstanding antiproliferative activity and selectivity shown by the most performant complexes do not seem a consequence of their superior internalisation in cancer cells, and are not always simply correlated with the ROS-induced production. Therefore, it is likely that a combination of factors and/or the ability of the complexes (of some of their components, including carbon monoxide) to interact with specific cellular target(s) is responsible for the observed anticancer activity. Although advanced and targeted experiments will be needed to advance the understanding of the mode of action, the proposed family of cationic triiron compounds appears really promising in view of developing optimal anticancer metal drugs, and an effort in this direction is recommended even by some ideal features: 1) the presence of an endogenous metal element; 2) the straightforward synthesis up to gram scale; 3) the avoidance of undesired side-reactions with common proteins; 4) the potential adjuvant effect of CO release; 5) the favourable and tuneable physico-chemical properties, and the wide opportunity for derivatisation offered by the vinyliminium ligand, as largely witnessed by previous findings.[22a]

Experimental

1) Materials and methods. Organic reactants (TCI Europe or Merck) and $[Fe_2Cp_2(CO)_4]$ (Strem) were commercial products of the highest purity available. Compounds **[1a,c,d,h,i]CF_3SO_3** and **[1h]NO_3**,[30,31] **[1b,e,f,g]CF_3SO_3**,[23] and **[2j]CF_3SO_3** [24a] were prepared according to the respective literature procedures, purified by alumina chromatography and checked for their purity by means of IR and ^{1}H NMR spectroscopy. Unless otherwise specified, operations were conducted in air. Chromatography separations were carried out on columns of deactivated alumina (Merck, 4% *w/w* water). Infrared spectra of solutions were recorded on a Perkin Elmer Spectrum 100 FT-IR spectrometer with a CaF_2 liquid transmission cell (2300-1500 cm^{-1} range). IR spectra of solid samples (650-4000 cm^{-1}) were recorded on a Perkin Elmer Spectrum One FT-IR spectrometer, equipped with a UATR sampling accessory. UV-Vis spectra (250-700 nm) were recorded on an Ultraspec 2100 Pro spectrophotometer using 1 cm PMMA cuvettes. IR and UV-Vis spectra were processed with Spectragryph software.[51] NMR spectra were recorded at 298 K on a Bruker Avance II DRX400 instrument equipped with a BBFO broadband probe. Chemical shifts (expressed in parts per million) are referenced to the residual solvent peaks[52] (^{1}H, ^{13}C) or to external standards[53] (^{14}N to CH_3NO_2). NMR spectra were assigned with the assistance of ^{1}H-^{13}C (*gs*-HSQC and *gs*-HMBC) correlation experiments.[54] NMR signals due to secondary isomeric forms (where it has been possible to detect them) are italicised. Elemental analyses were performed on a Vario MICRO cube instrument (Elementar). ESI mass spectra were acquired using a TripleTOF 5600$^+$ high-resolution mass spectrometer (Sciex, Framingham, MA, USA), equipped with a DuoSpray® interface operating with an ESI probe. GC analysis was performed on a Clarus 500 instrument (PerkinElmer) equipped with a 5 Å MS packed column (Supelco) and a TCD detector. Samples were analysed by isothermal runs (110 °C, 4 min) using He as carrier gas.

2) Synthesis and characterisation of compounds.

$[Fe_2Cp_2(CO)(\mu\text{-}CO)\{\mu\text{-}\eta^1\text{:}\eta^3\text{-}C^3(Fc)C^2HC^1N(R)(R')\}]CF_3SO_3$ (R = Me, R' = 2,6-C_6H_3ClMe, [2a]CF_3SO_3, Chart 2; R = Me, R' = 4-C_6H_4OMe, [2b]CF_3SO_3, Chart 3; R = Me, R' = 2-naphthyl, [2c]CF_3SO_3, Chart 4; R = Me, R' = CH_2Ph, [2d]CF_3SO_3, Chart 5; R = Me, R' = Cy, [2e]CF_3SO_3, Chart 6; R = Me, R' = $CH_2CH{=}CH_2$, [2f]CF_3SO_3, Chart 7; R = R' = CH_2Ph, [2g]CF_3SO_3, Chart 8; R = R' = Me, [2h]CF_3SO_3, Chart 9; R = Me, R' = 2,6-$C_6H_3Me_2$, [2i]CF_3SO_3, Chart 10).

General procedure. A solution of **[1a-i]CF_3SO_3** (ca. 1 mmol) in acetonitrile (10 mL) was treated with Me_3NO (1.3 eq.). The resulting mixture was stirred for 1 hour, during which time progressive colour darkening occurred. The complete conversion of the starting material into the corresponding acetonitrile adduct **[1'a-i]CF_3SO_3** (Scheme 1)[23,28] was checked by IR spectroscopy as it is routine for this type of synthesis.[24,25] The volatiles were removed under vacuum, thus the freshly obtained dark brown residue was dissolved into dichloromethane (ca. 20 mL). The solution was treated with ethynylferrocene (ca. 1.3 eq.), and the mixture was stirred at room temperature for 48 hours. The final solution was charged on an alumina column. Elution with CH_2Cl_2 and CH_2Cl_2/THF mixtures allowed to remove unreacted ethynylferrocene and impurities, then a fraction corresponding to the title product was collected using neat MeCN as eluent. Removal of the solvent under reduced pressure afforded a solid which was dissolved in the minimum volume of CH_2Cl_2; subsequent addition of hexane (30-50 mL) allowed the precipitation of a powder, which was dried under vacuum and stored in air. Compounds **[2h-i]CF_3SO_3** were previously obtained by a different procedure, which has been optimised here.[29] The syntheses of **[2b]CF_3SO_3** and **[2h]CF_3SO_3** were also carried out starting from 1 – 1.5 g of the respective aminocarbyne precursors, without a significant variation in the reaction yields.

Chart 1. Structure of [**2a**]$^+$.

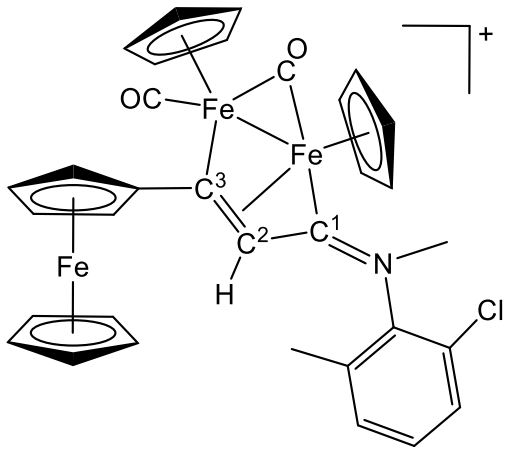

From **[1a]CF$_3$SO$_3$**. Dark brown solid, yield 81%. Anal. calcd. for $C_{34}H_{29}ClF_3Fe_3NO_5S$: C, 49.58; H, 3.55; N, 1.70; S, 3.89. Found: C, 49.67; H, 3.42; N, 1.62; S, 3.94. HR-ESI-MS: $[M]^+$ *m/z* = 673.99205 (theoretical for $[C_{33}H_{29}NClFe_3O_2]^+$: *m/z* = 673.99295; error: -1.3 ppm). IR (CH_2Cl_2): $\tilde{\upsilon}$/cm^{-1} = 1999vs (CO), 1818s (μ-CO), 1621m (C^1N). ^{1}H NMR (acetone-d_6): δ/ppm = 7.61 (d, ^3J = 7.7 Hz, 1 H, C_6H_3); 7.48 (t, ^3J = 8.4 Hz, 1 H, C_6H_3); 7.33 (d, ^3J = 8.3 Hz, 1 H, C_6H_3); 5.67, *5.65*, *5.38*, 5.36 (s, 10 H, Cp); 5.28 (s, 1 H, C^2H); 4.93, 4.71, 4.53, 4.28 (m, 4 H, C_5H_4); 4.43 (s, 3 H, NMe); 4.29 (s, 5 H, Cp^{Fc}); 1.97 (s, 3 H, C_6H_3*Me*). Conformer ratio (*cis*-E/*cis*-E) = 6. $^{13}C\{^1H\}$ NMR (acetone-d_6): δ/ppm = 253.3 (μ-CO); 234.9 (C^1); 210.6 (CO); 206.4 (C^3); 142.8 (*ipso*-C_6H_3); 134.4, 131.1, 130.9, 128.6, 128.2 (C_6H_3); 108.8 (*ipso*-C_5H_4); 92.4, 87.9 (Cp); 72.2, 69.2, 68.5, 67.7 (C_5H_4); 69.6 (Cp^{Fc}); 56.3 (C^2); 45.1 (NMe); 16.7 (C_6H_3*Me*). Crystals suitable for X-ray analysis were collected by slow diffusion at room temperature of diethyl ether into a dichloromethane solution of **[2a]CF$_3$SO$_3$**.

Chart 2. Structure of [**2b**]$^+$.

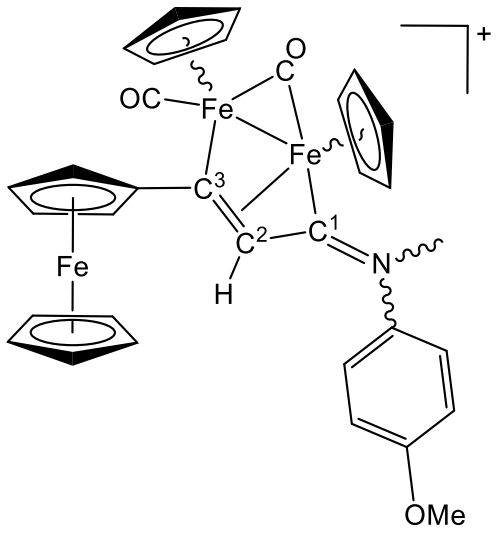

From **[1b]CF$_3$SO$_3$**. Dark-brown solid, yield 70%. Anal. calcd. for $C_{34}H_{30}F_3Fe_3NO_6S$: C, 50.72; H, 3.76; N, 1.74; S, 3.98. Found: C, 50.52; H, 3.83; N, 1.67; S, 4.03. HR-ESI-MS: $[M]^+$ *m/z* = 656.02548 (theoretical for $[C_{33}H_{30}Fe_3NO_3]^+$: *m/z* = 656.02684; error: -2.1 ppm). IR (CH_2Cl_2): ϋ/cm^{-1} = 1987vs (CO), 1813s (μ-CO), 1636m (C^1N). ***Cis*-[2b]CF$_3$SO$_3$**. ^{1}H NMR (acetone-d$_6$): δ/ppm = *7.69*, 7.33 (d, ^{3}J = 8.7 Hz, 2 H, C_6H_4); *7.26*, 7.02 (d, ^{3}J = 8.6 Hz, 2 H, C_6H_4); 5.56, 5.25, *5.22*, *5.15* (s, 10 H, Cp); 5.45 (s, 1 H, C^2H); 4.94, 4.69, 4.59, 4.55 (m, 4 H, C_5H_4); 4.46, *3.75* (s, 3 H, NMe); *4.47*, 4.31 (s, 5 H, Cp^{Fc}); *3.98*, 3.84 (s, 3 H, OMe). $^{13}C\{^1H\}$ NMR (acetone-d$_6$): δ/ppm = 255.2 (μ-CO); 228.4 (C^1); 210.4 (CO); 201.8 (C^3); 159.8, 139.5, 126.7, 122.6, 114.6, 114.4 (C_6H_4); 108.7 (*ipso*-C_5H_4); 91.9, 88.0, *87.6* (Cp); 72.1, 70.2, 68.9, 67.6 (C_5H_4); *69.6*, 69.4 (Cp^{Fc}); 56.1, *55.9* (C^2); 55.2, *54.1* (OMe); *52.2*, 45.9 (NMe). ***Trans*-[2b]CF$_3$SO$_3$**. ^{1}H NMR (acetone-d$_6$): δ/ppm = 7.58 (d, ^{3}J = 8.9 Hz, 2 H, C_6H_4); 7.07 (d, ^{3}J = 8.6 Hz, 2 H, C_6H_4); 4.98, 4.91 (s, 10 H, Cp); 4.45 (s, 3 H, NMe); 4.23 (s, 5 H, Cp^{Fc}); 3.82 (s, 3 H, OMe). $^{13}C\{^1H\}$ NMR (acetone-d$_6$): δ/ppm = 89.8 (Cp); 46.9 (NMe). *Cis*-E/*cis*-Z/*trans*-E ratio = 10:5:3.

Chart 3. Structure of [**2c**]$^+$.

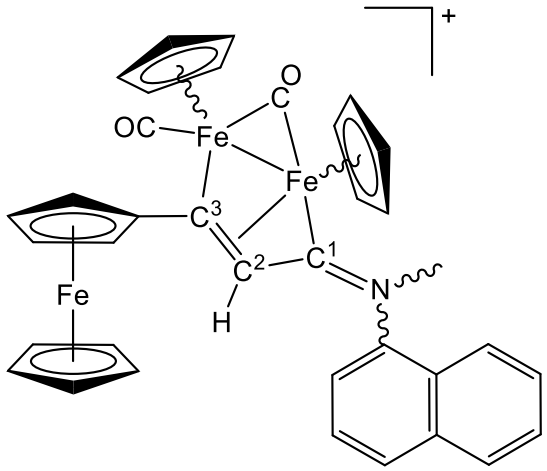

From **[1c]CF_3SO_3**. Dark-brown solid, yield 75%. Anal. calcd. for $C_{37}H_{30}F_3Fe_3NO_5S$: C, 53.85; H, 3.66; N, 1.70; S, 3.89. Found: C, 53.71; H, 3.61; N, 1.62; S, 3.80. HR-ESI-MS: $[M]^+$ *m/z* = 676.03146 (theoretical for $[C_{36}H_{30}Fe_3NO_2]^+$: *m/z* = 676.03192; error: -0.7 ppm). IR (CH_2Cl_2): ϋ/cm^{-1} = 1987vs (CO), 1814s (μ-CO), 1643w-m (C^1N). ***Cis*-[2c]CF_3SO_3**. ^1H NMR (acetone-d_6): δ/ppm =8.40-7.40 (m, 7 H, $C_{10}H_7$); 5.62, 5.30, *5.22*, *5.20* (s, 10 H, Cp); *5.77*, 5.61 (s, 1 H, C^2H); 4.96, *4.90*, *4.76*, 4.71, 4.69, *4.68*, *4.64*, 4.55 (m, 4 H, C_5H_4); 4.66, *3.91* (s, 3 H, NMe); *4.48*, 4.30 (s, 5 H, Cp^{Fc}). $^{13}C\{^1H\}$ NMR (acetone-d_6): δ/ppm = 254.9, *254.4* (μ-CO); 230.0, *228.5* (C^1); *210.6*, 210.4 (CO); *203.2*, 202.3 (C^3); 144.0-116.0 ($C_{10}H_7$); *109.1*, 108.7 (*ipso*-C_5H_4); 92.0, *91.9*, 88.1, *87.6* (Cp); *72.3*, 72.2, 68.9, *68.9*, *68.3*, 68.1, 67.6, *67.1* (C_5H_4); *69.6*, 69.4 (Cp^{Fc}); 56.4, *56.2* (C^2); *53.8*, 45.8 (NMe). ***Trans*-[2c]CF_3SO_3**. ^1H NMR (acetone-d_6): δ/ppm = 8.50-7.40 (m, 7 H, $C_{10}H_7$); *5.18*, 5.05, 4.97, *4.69* (s, 10 H, Cp); 4.66, *4.17* (s, 3 H, NMe); *4.48*, 4.21 (s, 5 H, Cp^{Fc}). $^{13}C\{^1H\}$ NMR (acetone-d_6): δ/ppm = 228.4, *226.5* (C^1); 209.5 (CO); 199.6 (C^3); 144.0-116.0 ($C_{10}H_7$); *90.1*, 89.9, 89.8, *89.7* (Cp); *70.3*, 70.2 (Cp^{Fc}); 52.6, *52.2* (C^2); *52.1*, 46.8 (NMe). *Cis*-E/*trans*-Z/*cis*-Z/*trans*-E ratio = 10:2:6:3.

Chart 4. Structure of [**2d**]$^+$.

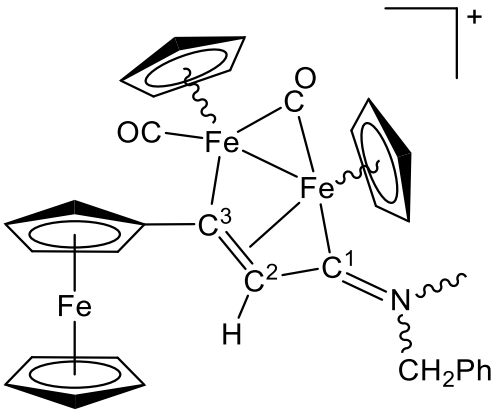

From **[1d]CF_3SO_3**. Dark-green solid, yield 94%. Anal. calcd. for $C_{34}H_{30}F_3Fe_3NO_5S$: C, 51.74; H, 3.83; N, 1.77; S, 4.06. Found: C, 51.50; H, 3.91; N, 1.67; S, 4.11. HR-ESI-MS: $[M]^+$ *m/z* = 640.03138 (theoretical for $[C_{33}H_{30}Fe_3NO_2]^+$: *m/z* = 640.03192; error: -0.8 ppm). IR (CH_2Cl_2): ϋ/cm^{-1} = 1987vs (CO), 1808s (μ-CO), 1666w-m (C^1N). ***Cis*-[2d]CF_3SO_3**. ^{1}H NMR (acetone-d_6): δ/ppm = 7.55-7.30 (m, 5 H, Ph); 5.71, 5.60 (d, $^2J_{HH}$ = 14 Hz, 2 H, CH_2); *5.53*, 5.48, *5.22*, 5.20 (s, 10 H, Cp); *5.53*, 5.23 (s, 1 H, C^2H); *4.96*, 4.94, *4.74*, 4.71, *4.57*, 4.56, 4.48, *4.42* (m, 4 H, C_5H_4); *4.43*, 4.34 (s, 5 H, Cp^{Fc}); 4.01, *3.20* (s, 3 H, NMe). $^{13}C\{^1H\}$ NMR (acetone-d_6): δ/ppm = *257.3*, 255.9 (μ-CO); 226.1 (C^1); 210.6 (CO); *202.1*, 201.4 (C^3); *133.3*, 132.9, 129.4-128.8 (Ph); 108.7, *108.6* (*ipso*-C_5H_4); *91.8*, 91.8, 87.6 (Cp); 72.4, *70.0*, *69.0*, 68.9, 68.1, *67.3*, 67.3 (C_5H_4); *69.5*, 69.5 (Cp^{Fc}); 61.4, *61.4* (CH_2); *54.5*, 54.3 (C^2); *47.6*, 42.9 (NMe). ***Trans*-[2d]CF_3SO_3**. ^{1}H NMR (acetone-d_6): δ/ppm = 7.55-7.30 (m, 5 H, Ph); 5.65-5.56 (m, 2 H, CH_2); 4.99, 4.88 (s, 10 H, Cp); 4.42 (s, 5 H, Cp^{Fc}); 4.05, *3.47* (s, 3 H, NMe). $^{13}C\{^1H\}$ NMR (acetone-d_6): δ/ppm = 253.5 (μ-CO); 224.6 (C^1); 210.0 (CO); 199.4 (C^3); 133.5, 129.4-126.7 (Ph); 89.9, *89.8*, 89.6, *89.5* (Cp); 70.0 (Cp^{Fc}); 62.7 (CH_2); *50.8*, 50.3 (C^2); *47.6*, 44.3 (NMe). *Cis*-E/*trans*-Z/*cis*-Z/*trans*-E ratio = 10:1:6:3.

Chart 5. Structure of [**2e**]$^+$.

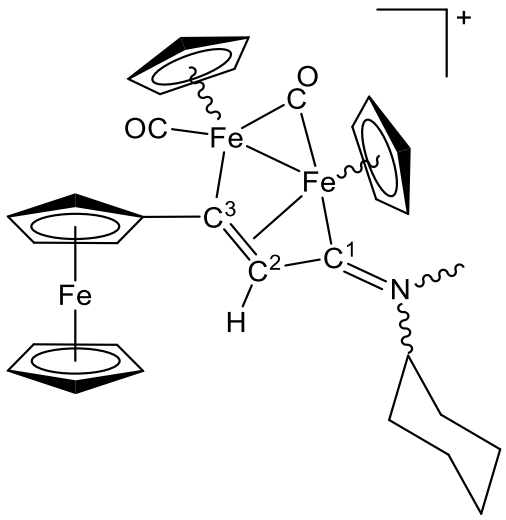

From **[1e]CF$_3$SO$_3$**. Dark-green solid, yield 94%. Anal. calcd. for $C_{33}H_{34}F_3Fe_3NO_5S$: C, 50.73; H, 4.39; N, 1.79; S, 4.11. Found: C, 50.62; H, 4.40; N, 1.85; S, 4.03. HR-ESI-MS: $[M]^+$ *m/z* = 632.06323 (theoretical for $[C_{32}H_{34}Fe_3NO_2]^+$: *m/z* = 632.06322; error: 0.0 ppm). IR (CH_2Cl_2): ϋ/cm^{-1} = 1988vs (CO), 1809s (μ-CO), 1656m (C^1N). ***Cis*-[2e]CF$_3$SO$_3$**. ^{1}H NMR (acetone-d$_6$): δ/ppm = *5.46*, 5.43 (s, 5 H, Cp); 5.44, *5.34* (s, 1 H, C^2H); *5.19*, 5.15 (s, 5 H, Cp'); *5.00–4.97* (m), 3.74 (tt, $^3J_{HH}$ = 11.9, 3.7 Hz) (1 H, NCH^{Cy}); *4.94*, 4.90 (dt, *J* = 2.5, 1.2 Hz, 1 H), 4.71 (dt, *J* = 3.4, 1.2 Hz, 1 H), 4.60–4.54 (m, 2 H) (C_5H_4); 4.40, *4.38* (s, 5 H, Cp^{Fc}); *3.99*, 3.30 (s, 3 H, NMe); 2.31 (d), 2.00–1.15 (m) (10 H, CH^{Cy}); Z/E ratio = 1.2. $^{13}C\{^1H\}$ NMR (acetone-d$_6$): δ/ppm = *257.1*, 256.0 (μ-CO); 224.1, *223.5* (C^1); 210.8, *210.6* (CO); 201.4, *201.3* (C^3); *108.7*, 108.4, (*ipso*-C_5H_4); 91.7, *91.6*, 87.6, *87.3* (Cp); 75.3, *68.2* (CH^{Cy}); 72.4, *72.3*, 68.9, *68.8*, *68.0*, 67.8, 67.4, *67.2* (C_5H_4); *69.5*, 69.4 (Cp^{Fc}); *53.9*, 53.0 (C^2); 43.2, *38.2* (NMe); 30.0, 29.9, 29.8, 29.8, 25.2, 24.8, 24.7, 24.6, 24.5 (CH_2^{Cy}). ***Trans*-[2e]CF$_3$SO$_3$**. ^{1}H NMR (acetone-d$_6$): δ/ppm = *5.86*, 5.79 (s, 1 H, C^2H); 4.96, *4.95* (s, 5 H, Cp); 4.85, *4.84* (s, 5 H, Cp'); 4.41 (s, Cp^{Fc}); 4.05, *3.50* (s, 3 H, NMe); E/Z ratio = 1.7. $^{13}C\{^1H\}$ NMR (acetone-d$_6$): δ/ppm = *90.2*, 89.8, 89.6, *89.4* (Cp); *70.2*, 70.1 (Cp^{Fc}); 40.3 (NMe). *trans*-*E*/*cis*-*E*/*trans*-*Z*/*cis*-*Z* ratio = 7:40:4:49.

Following a finer chromatographic purification using neat THF as eluent, a small amount of *E* isomers was isolated as a dark-green solid. ***Cis*-*Z*-[2e]CF$_3$SO$_3$**. ^{1}H NMR (acetone-d$_6$): δ/ppm = 5.45 (s, 1 H,

C^2H); 5.45, 5.17 (s, 10 H, Cp); 4.97, 4.92, 4.73, 4.57 (m, 4 H, C_5H_4); 4.58 (m, 1 H, CH^{Cy}); 4.42 (s, 5 H, Cp^{Fc}); 3.31 (s, 3 H, NMe); 2.33, 2.10-1.20 (m, 10 H, CH_2^{Cy}). $^{13}C\{^1H\}$ NMR (acetone-d_6): δ/ppm = 257.0 (μ-CO); 223.5 (C^1); 210.5 (CO); 201.4 (C^3); 91.6, 87.3 (Cp); 72.4, 68.9, 68.1, 67.2 (C_5H_4); 69.5 (Cp^{Fc}); 67.8 (CH^{Cy}); 54.0 (C^2); 43.1(NMe); 29.9, 29.8, 25.2, 24.8, 24.7 (CH_2^{Cy}). ***Trans*-Z-[2e]CF_3SO_3**. ^1H NMR (acetone-d_6): δ/ppm = 4.97, 4.85 (s, 10 H, Cp); 3.51 (s, 3 H, NMe). $^{13}C\{^1H\}$ NMR (acetone-d_6): δ/ppm = 89.8, 89.4 (Cp); 70.2 (Cp^{Fc}); 43.0 (NMe). *Cis*-Z/*trans*-Z ratio = 10.

Chart 6. Structure of [**2f**]$^+$.

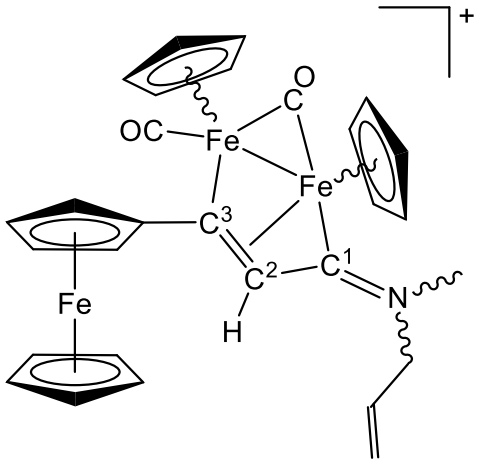

From **[1f]CF_3SO_3**. Dark-green solid, yield 82%. Anal. calcd. for $C_{30}H_{28}F_3Fe_3NO_5S$: C, 48.75; H, 3.82; N, 1.90; S. 4.34. Found: C, 48.66; H, 3.91; N, 1.87; S, 4.26. HR-ESI-MS: $[M]^+$ *m/z* = 590.01680 (theoretical for $[C_{29}H_{28}NFe_3O_2]^+$: *m/z* = 590.01627; error: 0.9 ppm). IR (CH_2Cl_2): ῡ/cm^{-1} = 1988vs (CO), 1809s (μ-CO), 1671m (C^1N). ***Cis*-[2f]CF_3SO_3**. ^1H NMR (acetone-d_6): δ/ppm = *6.10*, 5.79 (ddt, $^3J_{HH,trans}$ = 16.9 Hz, $^3J_{HH,cis}$ = 10.2 Hz, $^3J_{HH}$ = 6.1 Hz, 1 H, C*H*=CH_2); 5.49, *5.48*, 5.20, *5.19* (s, 10 H, Cp); *5.46*, 5.41 (s, 1 H, C^2H); 5.45-5.30 (m, 2 H, CH=C*H*$_2$); 5.09 (dd, $^2J_{HH}$ = 14.3 Hz, $^3J_{HH}$ = 6.8 Hz, 1 H, NCH_2); 5.00-4.90 (m, 1 H, NCH_2); *4.93*, 4.73, *4.59*, 4.58, 4.31, 4.29 (m, 4 H, C_5H_4); *4.42*, 4.40 (s, 5 H, Cp^{Fc}); 4.00, *3.36* (s, 3 H, NMe). $^{13}C\{^1H\}$ NMR (acetone-d_6): δ/ppm = *256.9*, 256.1 (μ-CO); 225.8

(C^1); 210.6 (CO); *201.5*, 201.3 (C^3); *130.8*, 130.0 (*C*H=CH_2); 121.6, *121.5* (CH=*C*H_2); 108.6, *108.5* (*ipso*-C_5H_4); 91.6, *91.6*, 87.5, *87.4* (Cp); 72.3, 68.9, 68.1, *67.2*, 66.9 (C_5H_4); 69.5 (Cp^{Fc}); 60.3 (NCH_2); *54.4*, 54.2 (C^2); *47.7*, 41.8 (NMe). ***Trans*-[2f]CF_3SO_3**. ^{1}H NMR (acetone-d_6): δ/ppm = 4.99, *4.98*, 4.88, *4.87* (s, 10 H, Cp); 4.05, *3.57* (s, 3 H, NMe). $^{13}C\{^1H\}$ NMR (acetone-d_6): δ/ppm = 89.8, *89.8*, 89.5, *89.4* (Cp); *70.2*, 70.1 (Cp^{Fc}). *Cis*-E/*trans*-Z/*cis*-Z/*trans*-E ratio = 10:1:7:2.

Following a finer chromatographic purification using a CH_2Cl_2/THF mixture (3:1 v/v) as eluent, a small amount of Z isomers was isolated as a dark-green solid. ***Cis*-Z-[2f]CF_3SO_3**. ^{1}H NMR (acetone-d_6): δ/ppm = 6.09 (m, 1 H, C*H*=CH_2); 5.64 (d, $^3J_{HH,trans}$ = 17.2 Hz, 1 H, CH=C*H*$_2$); 5.53 (d, $^3J_{HH,cis}$ = 10.4 Hz, 1 H, CH=C*H*$_2$); 5.48 (s, 1 H, C^2H); 5.48, 5.19 (s, 10 H, Cp); 5.09 (dd, $^2J_{HH}$ = 14.4 Hz, $^3J_{HH}$ = 6.1 Hz, 1 H, NCH_2); 4.95 (m, 1 H, NCH_2); 4.93, 4.73, 4.59, 4.58 (m, 4 H, C_5H_4); 4.42 (s, 5 H, Cp^{Fc}); 3.36 (s, 3 H, NMe). $^{13}C\{^1H\}$ NMR (acetone-d_6): δ/ppm = 256.7 (μ-CO); 225.8 (C^1); 210.5, (CO); 201.5 (C^3); 130.8 (*C*H=CH_2); 121.4 (CH=*C*H_2); 91.7, 87.4 (Cp); 72.3, 68.9, 68.1, 67.2 (C_5H_4); 69.5 (Cp^{Fc}); 60.3 (NCH_2); 54.5 (C^2); 47.7 (NMe). ***Trans*-Z-[2f]CF_3SO_3**: ^{1}H NMR (acetone-d_6): δ/ppm = 4.98, 4.87 (s, 10 H, Cp); 3.57 (s, 3 H, NMe). $^{13}C\{^1H\}$ NMR (acetone-d_6): δ/ppm = 89.8, 89.4 (Cp); 70.2 (Cp^{Fc}); 61.6 (NCH_2); 54.3 (C^2); 47.3 (NMe). *Cis*-Z/*trans*-Z ratio = 5.

Chart 7. Structure of [**2g**]$^+$.

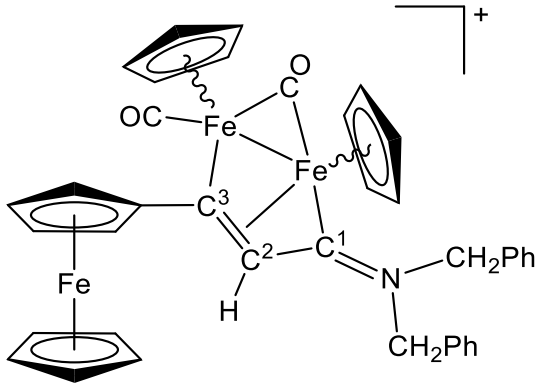

From **[1g]CF$_3$SO$_3$**. Dark-green solid, yield 80%. Anal. calcd. for $C_{40}H_{34}F_3Fe_3NO_5S$: C, 55.52; H, 3.96; N, 1.62; S. 3.71. Found: C, 55.70; H, 4.02; N, 1.68; S, 3.60. HR-ESI-MS: $[M]^+$ *m/z* = 716.06323 (theoretical for $[C_{39}H_{34}Fe_3NO_2]^+$: *m/z* = 716.06322; error: 0.0 ppm). IR (CH_2Cl_2): ϋ/cm^{-1} = 1986s (CO), 1809s (μ-CO), 1638m (C^1N). ^{1}H NMR (acetone-d_6): δ/ppm = 7.53–7.47 (m, 5 H), 7.42–7.35 (m, 3 H), 7.23–7.16 (m, 2 H) (Ph); *5.95*, 5.92 (d, $^2J_{HH}$ = 15 Hz, 1 H); 5.64, *5.62* (d, $^2J_{HH}$ = 15 Hz, 1 H) (NCH_2); 5.54, *4.91* (s, 5H, Cp); 5.26, *4.73* (s, 5 H, Cp'); 5.16* (s, 1 H, C^2H); *4.97–4.95*, 4.93–4.91 (m, 1 H), 4.72–4.71, *4.68–4.66* (m, 1 H) (C_5H_4); *4.59*, 4.55 (s, 1 H, NCH_2'); 4.57–4.54 (m, 1 H, C_5H_4); 4.53, *4.50* (s, 1 H, NCH_2'); 4.42 (dt, *J* = 2.5, 1.3 Hz, 1 H, C_5H_4); *4.40*, 4.27 (s, 5 H, Cp^{Fc}). *Cis*/*trans* ratio = 6.5. *Isochronous for both isomers. $^{13}C\{^1H\}$ NMR (acetone-d_6): δ/ppm = 256.6 (μ-CO); 227.2 (C^1); 210.5, (CO); 202.2 (C^3); 133.0, 132.7, 129.6, 129.5, 129.2, 129.0 (Ph); 109.0 (*ipso*-C_5H_4); 92.1, *89.9*, *89.7*, 87.7 (Cp); 72.5, 69.8, 68.4, 67.4 (C_5H_4); *70.0*, 69.8 (Cp^{Fc}); 62.7, 61.1 (CH_2); 54.8 (C^2).

Chart 8. Structure of [**2h**]$^+$.[29]

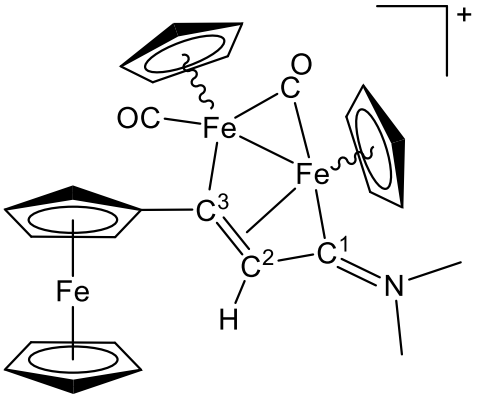

From **[1h]CF$_3$SO$_3$**. Green solid, yield 93%. Anal. calcd. for $C_{28}H_{26}F_3Fe_3NO_5S$: C, 47.16; H, 3.67; N, 1.96; S, 4.50. Found: C, 47.28; H, 3.76; N, 2.01; S, 4.41. IR (solid state): ϋ/cm^{-1} = 3103br-w, 2941vw, 1973s (CO), 1797s (μ-CO), 1683m (C^1N), 1453w, 1435w, 1417w-m, 1384w, 1360w, 1260vs, 1223m-s, 1150s, 1106w-m, 1058w-m, 1045w-m, 1029vs, 1003sh, 828br-s, 784m, 754w-m, 677m-s, 653w. IR

(CH_2Cl_2): ῡ/cm^{-1} = 1988vs (CO), 1805s (μ-CO), 1690w-m (C^1N). ^1H NMR (acetone-d_6): δ/ppm = 5.47, 5.16, *4.98*, *4.86* (s, 10 H, Cp); 5.39 (s, 1 H, C^2H); 4.93, 4.73, 4.58, 4.56 (m, 4 H, C_5H_4); *4.43*, 4.41 (s, 5 H, Cp^{Fc}); *4.07*, 4.03, *3.64*, 3.44 (s, 6 H, NMe_2). Cis/trans ratio = 5.

Chart 9. Structure of [**2i**]$^+$.[29]

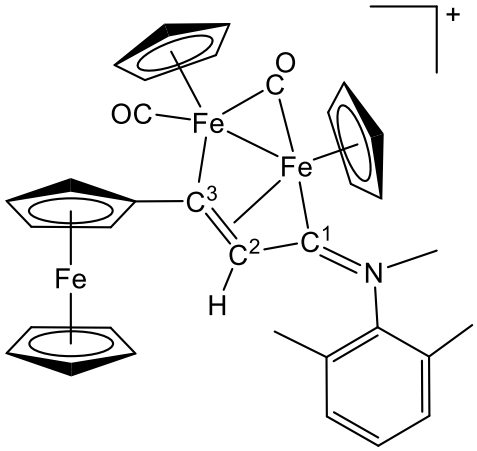

From **[1i]CF_3SO_3**. Green-brown solid, yield 81%. Anal. calcd. for $C_{35}H_{32}F_3Fe_3NO_5S$: C, 52.34; H, 4.02; N, 1.74; S, 3.99. Found: C, 52.20; H, 4.11; N, 1.67; S, 4.10. Yield: 230 mg, 81%. IR (CH_2Cl_2): ῡ/cm^{-1} = 2000vs (CO), 1816s (μ-CO), 1629m (C^1N). ^1H NMR (acetone-d_6): δ/ppm = 7.35-7.10 (m, 3 H, C_6H_3); 5.65, 5.37 (s, 10 H, Cp); 5.00 (s, 1 H, C^2H); 4.98, 4.69, 4.52, 4.30 (s, 4 H, C_5H_4); 4.43 (s, 3 H, NMe); 4.23 (s, 5 H, Cp^{Fc}); 2.51, 1.89 (s, 6 H, C_6H_3*Me_2*).

[Fe_2Cp_2(CO)(μ-CO){μ-$η^1$:$η^3$-C^3(Fc)$C^2HC^1NMe_2$}]NO_3, [2h]NO_3 (Chart 11).

Chart 10. Structure of [**2h**]$^+$.

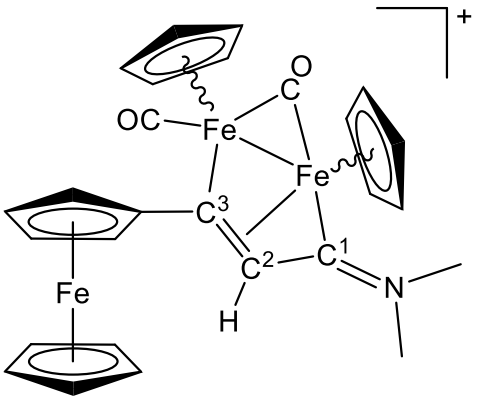

A solution of **[1h]NO$_3$** (200 mg, 0.450 mmol) in acetonitrile (15 mL) was treated with Me_3NO (44 mg, 0.59 mmol), and the resulting mixture was stirred for 2 hours. The complete conversion of [**1h**]NO_3 into the acetonitrile adduct $[Fe_2Cp_2(CO)(\mu\text{-}CO)(NCMe)\{\mu\text{-}CNMe_2\}]NO_3$ was checked by IR spectroscopy [IR (MeCN): $\tilde{\upsilon}/cm^{-1}$ = 1984vs (CO), 1812s (μ-CO), 1589m (μ-CN)]. The volatiles were removed under vacuum, thus the dark brown residue was dissolved into dichloromethane (20 mL). The dichloromethane solution was treated with ethynylferrocene (125 mg, 0.595 mmol), and the mixture was stirred at room temperature for 72 hours. The final solution was charged on an alumina column. A fraction corresponding to the title product was collected using a MeCN/MeOH mixture (95:5 v/v) as eluent. Removal of the solvent under reduced pressure afforded a solid which was dissolved in the minimum volume of CH_2Cl_2; subsequent addition of hexane (30 mL) allowed the precipitation of a powder, which was dried under vacuum and stored in air. Dark-green solid, yield 203 mg (72%). Anal. calcd. for $C_{27}H_{26}Fe_3N_2O_5$: C, 51.80; H, 4.19; N, 4.47. Found: C, 51.68; H, 4.23; N, 4.46. HR-ESI-MS: $[M]^+$ *m/z* = 563.99894 (theoretical for $[C_{27}H_{26}Fe_3NO_2]^+$: *m/z* = 564.00062; error: -3.0 ppm). IR (solid state): $\tilde{\upsilon}/cm^{-1}$ = 3358br, 3086w-m, 2973w, 2935w, 2868w, 2209w, 2172w-m, 1960vs (CO), 1787vs (μ-CO), 1686s (C^1N), 1634sh, 1449w, 1435w, 1415m, 1381m, 1338br-s (NO_3^-), 1261w, 1226w-m, 1191w, 1143w, 1116sh, 1105m, 1043m, 1023m, 1002m, 948vw, 830s, 783m-s, 729w, 676m-s, 652w. IR (CH_2Cl_2): $\tilde{\upsilon}/cm^{-1}$ = 1987vs (CO), 1805s (μ-CO), 1692m (C^1N). ^1H NMR (acetone-d_6): δ/ppm =

5.51, 5.15, *4.96*, *4.89* (s, 10 H, Cp); 5.45 (s, 1 H, C^2H); 4.95, 4.70, 4.55 (m, 4 H, C_5H_4); 4.45, *4.44* (s, 5 H, Cp^{Fc}); *4.07*, 4.03, *3.62*, 3.47 (s, 6 H, NMe). ^{14}N NMR (acetone-d_6): δ/ppm = -1.5 (s, $\Delta\nu_{1/2}$ = 126 Hz, NO_3^-). Cis/trans ratio = 5.

Synthesis of $[Fe_2Cp_2(CO)(\mu\text{-}CO)\{\mu\text{-}\eta^1\text{:}\eta^3\text{-}C^3(Fc)C^2HC^1(CN)NMe_2\}]$, 3 (Chart 12).

Chart 11. Structure of **3**.

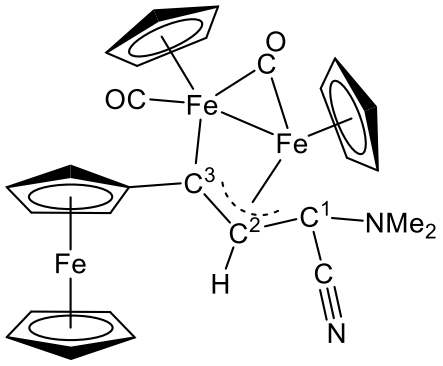

A solution of **[2h]CF_3SO_3** (250 mg, 0.351 mmol) in CH_2Cl_2 (20 mL) was treated with tetrabutylammonium cyanide (113 mg, 0.421 mmol), and the mixture was stirred at room temperature for 45 minutes, under the protection of N_2 atmosphere. The final mixture was charged on an alumina column, and subsequent chromatography was carried out under N_2 atmosphere. Thus, hexane and hexane/diethyl ether mixtures were used to elute impurities, then a brown fraction corresponding to **3** was collected with diethyl ether. Solvent evaporation afforded an oily residue. Dissolution into CH_2Cl_2 (ca. 5 mL) followed by pentane addition (ca. 20 mL) allowed to obtain a dark-brown air-stable powder, which was dried under vacuum. Yield 145 mg, 70%. Anal. calcd. for $C_{28}H_{26}Fe_3N_2O_2$: C, 56.99; H, 4.44; N, 4.75. Found: C, 56.85; H, 4.58; N, 4.69. HR-ESI-MS: $[M+H]^+$ *m/z* = 591.01075 (theoretical for $[C_{28}H_{26}Fe_3N_2O_2+H]^+$: *m/z* = 591.01152; error: -1.3 ppm). IR (CH_2Cl_2): $\tilde{\upsilon}/cm^{-1}$ = 2188m (C≡N), 1967vs (CO), 1787s (μ-CO). ^1H NMR (acetone-d_6): δ/ppm = 5.42 (s, 1 H, C^2H); 4.87, 4.72 (s, 10 H, Cp); 4.86, 4.61, 4.48, 4.34 (m, 4 H, C_5H_4); 4.39 (s, 5 H, Cp^{Fc}); 2.33, 1.80 (s, 6 H, NMe_2). $^{13}C\{^1H\}$

NMR (acetone-d_6): δ/ppm = 264.0 (μ-CO); 213.8 (CO); 194.9 (C^3); 120.1 (C≡N); 111.9 (*ipso*-C_5H_4); 89.5, 85.7 (Cp); 83.3 (C^2); 72.3, 67.4, 67.3, 66.8 (C_5H_4); 68.9 (Cp^{Fc}); 65.9 (C^1); 49.1, 41.6 (NMe_2). Crystals suitable for X-ray analysis were collected by slow diffusion of pentane into a dichloromethane solution of **3**, settled aside at –30°C.

Synthesis of [FeCp(CO){C^1N(Me)(Xyl)C^2HC^3(Fc)C(=O)}], 4 (Chart 13).[29]

Chart 12. Structure of **4**.

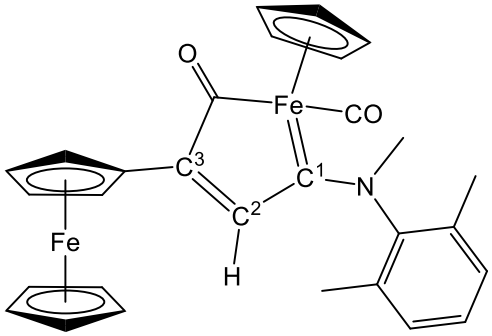

An optimised procedure with respect to the literature is reported. A solution of **[2i]CF_3SO_3** (256 mg, 0.319 mmol) in THF (15 mL) was treated with pyrrolidine (0.26 mL, 3.1 mmol). The mixture was left stirring for 19 hours, during which progressive colour turning from brown to red and then to violet was observed. The final solution was filtered on an alumina pad by using THF as eluent. The volatiles were removed under reduced pressure. The resulting residue was dissolved in CH_2Cl_2, and some alumina was added to the solution. After solvent removal under reduced pressure, the solid residue was charged on an alumina column. Hexane and hexane/diethyl ether mixtures were used to elute impurities. A violet band corresponding to **4** was collected with CH_2Cl_2. Solvent evaporation afforded an oily residue, which was dissolved in CH_2Cl_2 (ca. 3 mL) and treated with pentane (ca. 20 mL). The product was obtained as a violet powder upon removal of the solvent under vacuum. Yield 120 mg (71%). Anal. calcd. for $C_{29}H_{27}Fe_2NO_2$: C, 65.32; H, 5.10; N, 2.63. Found: C, 65.12; H, 5.18; N, 2.71. IR (CH_2Cl_2): ϋ/cm^{-1} = 1913vs (CO), 1593m (CO_{acyl}). IR (THF): ϋ/cm^{-1} = 1914vs (CO), 1595m (CO_{acyl}).

^{1}H NMR (acetone-d_6): δ/ppm = 7.35-7.28 (m, 3 H, C_6H_3); 6.82 (s, 1 H, C^2H); 4.85, 4.48, 4.36, 4.33 (m, 4 H, C_5H_4); 4.70, 4.03 (s, 10 H, Cp); 3.88 (s, 3 H, NMe); 2.30, 2.21 (s, 6 H, $C_6H_3Me_2$).

3) X-ray crystallography.

Crystal data and collection details for **[2a]CF_3SO_3** and **3** are reported in Table 6. Data were recorded on a Bruker APEX II diffractometer equipped with a PHOTON100 detector using Mo–Kα radiation. Data were corrected for Lorentz polarisation and absorption effects (empirical absorption correction SADABS).[55] The structures were solved by direct methods and refined by full-matrix least-squares based on all data using F^2.[56] Hydrogen atoms were fixed at calculated positions and refined by a riding model. All non-hydrogen atoms were refined with anisotropic displacement parameters.

Table 6. Crystal data and measurement details for **[2a]CF_3SO_3** and **3**.

	[2a]CF_3SO_3	**3**
Formula	$C_{34}H_{29}ClF_3Fe_3NO_5S$	$C_{28}H_{26}Fe_3N_2O_2$
FW	823.64	590.06
T, K	100(2)	100(2)
λ, Å	0.71073	0.71073
Crystal system	Monoclinic	Monoclinic
Space group	$P2_1/c$	$P2_1/n$
a, Å	13.9821(11)	9.9211(7)
b, Å	15.0395(12)	18.5237(13)
c, Å	14.8640(11)	13.2560(9)
β,°	98.152(3)	94.731(2)
Cell Volume, Å^3	3094.1(4)	2427.8(3)
Z	4	4
D_c, g·cm^{-3}	1.768	1.614
μ, mm^{-1}	1.606	1.798
F(000)	1672	1208
Crystal size, mm	0.25×0.18×0.12	0.16×0.15×0.12
θ limits,°	1.936–25.998	1.893-25.995
Reflections collected	41387	30955
Independent reflections	6091 [R_{int} = 0.1119]	4770 [R_{int} = 0.0634]
Data / restraints /parameters	6091 / 40 / 441	4770 / 6 / 318

Goodness on fit on F^2	1.038	0.990
R_1 ($I > 2\sigma(I)$)	0.0418	0.0458
wR_2 (all data)	0.1167	0.1257
Largest diff. peak and hole, e Å^{-3}	1.045 / –0.518	1.742 / –0.911

4) Solubility and stability in aqueous media, carbon monoxide release (Table 2)

a) Solubility in water (D_2O). Each iron compound was added to a D_2O solution (0.7 mL) of Me_2SO_2 (c = $3.3 \cdot 10^{-3}$ mol·L^{-1}) and the resulting mixture was stirred at 21 °C for 30 minutes. The saturated solution was filtered over celite, transferred into an NMR tube and analysed by ^{1}H NMR spectroscopy. The concentration (*i.e.,* solubility) was calculated by the relative integral with respect to Me_2SO_2 as internal standard [δ/ppm = 3.06].

b) Stability in water/methanol and water/DMSO solution. Solutions of [**2a-i**]$^+$ were prepared by dissolving the analysed compound (*ca*. 4 mg) in CD_3OD (0.5 mL), then adding a D_2O solution (0.5 mL) containing Me_2SO_2 as internal standard. A 3:1 *v*/*v* CD_3OD/D_2O solution was prepared for **3** and **4**. The final mixture was filtered over celite, and the solution was transferred into an NMR tube. The solution was analysed by ^{1}H NMR and subsequently heated at 37 °C for 72 h. After cooling to room temperature, the final solutions were separated from a minor amount of brown precipitate by celite filtration and analysed by ^{1}H NMR. The residual amount of starting material was calculated with respect to Me_2SO_2. Data related to the complexes at 0 h are reported in the Supporting Information and referenced to the Me_2SO_2 peak as in pure CD_3OD [δ/ppm = 3.14]. Analogous experiments were carried out with D_2O/DMSO-d_6 mixtures.

c) Stability in cell culture medium/methanol solution. Deuterated cell culture medium (DMEM-d) was prepared using powdered DMEM cell culture medium (1000 mg/L glucose and L-glutamine, without sodium bicarbonate and phenol red; D2902 - Merck), D_2O (10 mg/mL), Me_2SO_2 as internal standard

($6.6 \cdot 10^{-3}$ M) and NaH_2PO_4 / Na_2HPO_4 as buffer (0.10 M, pD = 7.5 [57]). Solutions of iron complexes were prepared, treated and analysed by NMR as described at point b).

d) CO release in water/methanol solution. In a 15x45 mm screw neck glass vial (5.0 mL total volume), the selected compound was accurately weighted (*ca.* 4 mg), dissolved in the appropriate MeOH/water mixture as in the related NMR experiments (4.0 mL total liquid volume; $c_{complex} \approx 1.2 \cdot 10^{-3}$ mol·L^{-1}). Next, the vial was sealed with a PTFE/silicone septum screw cap and maintained at 37 °C for 24 h, by full immersion into a thermostated water bath. After cooling to room temperature, the headspace was sampled with a gas-tight microsyringe (250 μL) and analysed by GC-TCD. Measurements were performed in duplicate or triplicate for each compound. The amount of carbon monoxide (n_{CO}, mmol) was calculated based on a calibration curve obtained from analyses of known CO/air mixtures (0.1-1.0 mmol·L^{-1}), assuming ideal gas behaviour. The number of equivalents of carbon monoxide released ($eq_{CO} = n_{CO}/n_{complex}$) was calculated with respect to the initial amount of the complex.

5) Determination of partition coefficients (Log P_{ow})

Partition coefficients (P_{ow}), defined as $P_{ow} = c_{org}/c_{aq}$, where c_{org} and c_{aq} are the molar concentrations of the selected compound in the n-octanol and aqueous phases, respectively, were determined by the shake-flask method and UV-Vis measurements, according to a previously described procedure.[58] All the operations were carried out at 21 ± 1°C. The wavelength of the maximum absorption of each compound in the 280-360 nm range was used for UV-Vis quantitation. Log P_{ow} values are compiled in Table 2.

6) Electrochemistry

Cyclic voltammetry measurements were performed with a PalmSens4 instrument interfaced to a computer employing PSTrace5 electrochemical software. All potentials refer to $FeCp_2$. HPLC grade DMSO (Merck) was stored under Ar over 3Å molecular sieves. $[N^nBu_4]PF_6$ (Fluka, electrochemical grade) and $FeCp_2$ (Fluka) were used without further purification. CV measurements were carried out under Ar using 0.1 M $[N^nBu_4]PF_6$ in DMSO as the supporting electrolyte. The working and the counter electrodes consisted of a Pt disk and a Pt gauze, respectively, both sealed in a glass tube. An Ag/AgCl, KCl sat electrode was employed as a reference. The three-electrode home-built cell was pre-dried by heating under vacuum and filled with argon. The Schlenk-type construction of the cell maintained anhydrous and anaerobic conditions. The solution of supporting electrolyte, prepared under argon, was introduced into the cell and the CV of the solvent was recorded. The analyte was then introduced and voltammograms were recorded. Under the present experimental conditions, the one-electron reduction of ferrocene occurred at E° = +0.56 V *vs* Ag/AgCl, KCl sat. Phosphate buffer solutions (Na_2HPO_4/KH_2PO_4, ΣcPO_4 = 50 mM, pH = 6.7) were prepared in ultrapure H_2O and used as supporting electrolytes for the measurements in aqueous media at a Teflon encapsulated carbon-glassy working electrode. Prior to measurements, the glassy carbon working electrode was polished according to the following procedure: manual rubbing with 0.3 μm Al_2O_3 slurry in water (eDAQ) for 2 min, then sonication in ultrapure water for 10 min, manual rubbing with 0.05 μm Al_2O_3 slurry in water (eDAQ) for 2 min, then sonication in ultrapure water for 10 min. The supporting electrolyte was introduced into the electrochemical cell and deaerated by argon bubbling for some minutes. Infrared (IR) spectroelectrochemical measurements were carried out using an optically transparent thin-layer electrochemical (OTTLE) cell equipped with CaF_2 windows, platinum mini-grid working and auxiliary electrodes and silver wire pseudo-reference electrode.[59] During the microelectrolysis procedures, the electrode potential was controlled by a PalmSens4 instrument interfaced to a computer employing PSTrace5 electrochemical software. Argon-saturated DMSO solutions of the analysed compound,

containing $[N^nBu_4]PF_6$ 0.1 M as the supporting electrolyte, were used. The *in situ* spectroelectrochemical experiments were performed by collecting IR spectra at fixed time intervals during the oxidation or reduction, obtained by continuously increasing or lowering the initial working potential at a scan rate of 1.0 mV/sec.

7) Cell culture and cytotoxicity studies

In vitro cytotoxicity investigations were carried out by using human ovarian carcinoma cisplatin-sensitive A2780 (ECACC93112519), human ovarian carcinoma cisplatin resistant A2780cisR (ECACC 93112517), human pancreas adenocarcinoma BxPC-3 (ATCC CRL-1687) and mouse embryo fibroblasts Balb/3T3 clone A31 (ATCC CCL-163) cell lines. A2780 and A2780cisR were purchased from the European Collection of Authenticated Cell Cultures (ECACC), and BxPC-3 and Balb/3T3 clone A31 cell lines from the American Type Culture Collection (ATCC). The cell lines were propagated as indicated by the supplier in RPMI 1640 (Merck- A2780, A2780cisR and BxPC-3) containing 2 mM of L-glutamine (Merck), 1% of penicillin/streptomycin solution (Merck-10,000 U ml-1:10 mg ml-1), 10% of foetal bovine serum (Merck-FBS) and antimycotic. The acquired resistance of A2780cisR cells was maintained by routine supplementation of media with 1 μM of cisplatin and the BxPC-3 medium was also supplemented with 1% of sodium pyruvate (Merck). Balb/3T3 clone A31 cells were routinely cultured in Dulbecco's modified Eagle medium (Merck-DMEM) supplemented with 4 mM of L-glutamine, 1% of penicillin/streptomycin solution, 10% of calf serum (Merck) and antimycotic. The cells were maintained under standard tissue culture conditions of 37 °C and 5% atmosphere of CO_2. A2780, A2780cis, BxPC-3 and Balb/3T3 clone A31 cells were seeded into 96-well culture plates at a concentration of $3{\cdot}10^3$, $6{\cdot}10^3$, $7{\cdot}10^3$ and $1{\cdot}10^3$ cells per well, respectively. Stock solutions of compounds were prepared in DMSO and were diluted in medium; the solutions were sequentially diluted to give a final DMSO concentration of ≤1% and a final compound concentration

range (0−100 μM). After overnight incubation, the cells were treated with different concentrations (0–100 μM) of the selected compounds for 72 hours. Then the cell viability was investigated by means of WST-1 tetrazolium salt reagent. Briefly, the cells were incubated for 4 hours with WST-1 reagent diluted 1:10, at 37 °C and 5% CO_2. Measurements of formazan dye absorbance were carried out with a microplate reader (Biorad, Milan, Italy) at 450 nm, using 655 nm as the reference wavelength. The 50% inhibitory concentration of tested compound (IC_{50}) refers to the concentration at which 50% of cell death is observed with respect to the control. All the in vitro biological tests were performed in triplicate. Concentration effect curves were generated by nonlinear regression curves (GraphPad Prism) and the data are reported as mean ± standard deviation.

8) Iron uptake assessment

A2780 and Balb/3T3 clone A31 cells were allowed to proliferate for 24 h before being incubated for 24 h in a complete medium containing 10 μM of [**2a**]CF_3SO_3, [**2f**]CF_3SO_3 and [**2h**]NO_3, respectively. At the end of the uptake period, cells were quickly washed three times with DPBS, collected, counted and gently spun down (400 g for 5 min), and processed for subsequent ICP-AES analysis. The determination of metal concentration in the selected cancer cell line was performed according to a well-established protocol[60,61] using a Varian 720-ES inductively coupled plasma atomic emission spectrometer (ICP-AES) equipped with a CETAC U5000 AT+ ultrasonic nebuliser, to increase the method sensitivity. Each sample of the cellular pellet was recovered in a PE vial and mineralised in a thermo-reactor at 80 °C for 8 h with 2 mL of 50% v/v diluted aqua regia (HCl suprapure grade and HNO_3 suprapure grade in a 3:1 ratio) in Milli-Q water (≥18 MΩ · cm). After that time, the samples were cooled down to room temperature and further diluted with 4 mL of ultrapure water (≥18 MΩ · cm). All the samples were spiked with 1 ppm of Ge used as an internal standard and analysed.

Calibration standards were prepared by gravimetric serial dilution from a commercial standard solution of iron at 1000 $mg \cdot L^{-1}$. The wavelength used for iron was 238.204 nm, whereas for Ge the line at 209.426 nm was used. The operating conditions were optimised to obtain maximum signal intensity and, between each sample, a rinsed solution of HCl suprapure grade and HNO_3 suprapure grade at a 3:1 ratio was used to avoid any "memory effect". The iron content normally presents in the cells was determined using non-treated cells and subtracted to all the other samples. Finally, iron concentration was normalised to the cell number.

9) ROS production

The intracellular increase of reactive oxygen species (ROS) upon treatment of the analysed compounds was measured by using the DCFH-DA (2',7'-dichlorodihydrofluorescein diacetate, Merck) assay, based on cellular uptake of the non-fluorescent diacetate following deacetylation by esterases (2',7'-dichlorodihydrofluorescein, DCFH) and oxidation to the fluorescent dichlorofluorescein (2',7'-dichloro-fluorescein, DCF). A2780, A2780cisR and Balb/3T3 clone A31 cells were seeded at a concentration of $4 \cdot 10^4$, $4 \cdot 10^4$ and $2 \cdot 10^4$ cells/well/90 µL of complete growth medium into 96-well plates, respectively. After overnight incubation, the cells were treated following manufacturer protocol. The culture medium was supplemented with 100 mL of a solution containing the fluorogenic probe and cells were incubated with 5% CO_2 at 37 °C. After 1 h, cells were exposed with a final concentration of 10 µM of the tested compound and 5% CO_2 at 37 °C; H_2O_2 and menadione 100 µM [62] were used as a positive control. Stock solutions of compounds were prepared as described above; cells incubated with comparable concentration of DMSO in supplemented cell culture medium were used as negative control. The fluorescence was measured up to 24 hours with an excitation wavelength of 485 nm and with a 535 nm emission filter by Multilabel Counter (PerkinElmer, Waltham, USA). The analyses were conducted in triplicate and experimental data were reported as mean ± SD. Statistical differences were analysed

using one-way analysis of variance (ANOVA), and a Tukey test was used for post hoc analysis. A p-value <0.05 was considered statistically significant.

10) Interaction with biomolecules.

a) Sample preparation. All the selected proteins and the oligonucleotide ODN2 were purchased from Merck and used as received; the thioredoxin reductase model **TrxR-pept** was synthesised according to the literature.[49] The stock solutions of the selected iron complexes were freshly prepared in DMSO to a final concentration of 10^{-2} M. Stock solution of **TrxR-pept** was prepared in LC-MS grade water by simply dissolving the required amount of lyophilised peptide to reach a final concentration of 10^{-3} M. Stock solutions of bovine serum albumin (BSA), cytochrome c (Cyt c), hen egg-white lysozyme (HEWL), ubiquitin (Ub), superoxide dismutase (SOD) and human carbonic anhydrase I (hCA I), were prepared in 2 mM ammonium acetate solution, pH 6.8, at 10^{-3} M. The stock solution of the oligonucleotide ODN2 was prepared in LC-MS grade water at 10^{-3} M.

Regarding the interaction tests with **TrxR-pept**, appropriate aliquots of each iron compound and **TrxR-pept** stock solutions were mixed and diluted with LC-MS grade water to 10^{-4} M final concentration and a **TrxR-pept**/complex ratio of 1.1.

For each **[2a]CF_3SO_3**/protein pair, appropriate aliquots of these stock solutions were mixed and diluted with 2 mM ammonium acetate solution (pH 6.8) to a final protein concentration of 10^{-4} M and a protein-to-metal complex molar ratio of 1:3.

In the case of **[2a]CF_3SO_3**/ODN2 pair, appropriate aliquots of the respective stock solutions were mixed and diluted with LC-MS grade water to a final ODN concentration of 10^{-4} M and an oligonucleotide-to-metal complex molar ratio of 1:3.

All the mixtures were incubated for 24 h at 37 °C. After the incubation time, opportune dilutions were performed as follows. **TrxR-pept** solutions were further diluted with LC-MS grade water to a final

dodecapeptide concentration of $5 \cdot 10^{-6}$ M, and added with 0.1% v/v of formic acid just before infusion into the mass spectrometer. The protein solutions were diluted with 2 mM ammonium acetate solution (pH 6.8) to a final protein concentration of 10^{-6} M, and added with 0.1% v/v of formic acid just before infusion. The ODN2 solution was diluted with LC-MS grade water to a final concentration of 10^{-5} M, and added with 1% v/v of triethylamine just before infusion.

b) HR-ESI-MS instrumental parameters. The ESI mass spectra were acquired using a TripleTOF® 5600^+ high-resolution mass spectrometer (Sciex, Framingham, MA, USA), equipped with a DuoSpray® interface operating with an ESI probe. ESI mass spectra were acquired through direct infusion at 7 μL min^{-1} flow rate. The ESI source parameters were optimised for each biomolecule and were as follows: for **TrxR-pept** positive polarity, ionspray voltage floating 5500 V, temperature 25 °C, ion source gas 1 (GS1) 35 $L \cdot min^{-1}$; ion source gas 2 (GS2) 0 $L \cdot min^{-1}$; curtain gas (CUR) 20 L min^{-1}, declustering potential (DP) 300 V, collision energy (CE) 10 V, acquisition range 1100–1600 *m/z*; for BSA positive polarity, ionspray voltage floating 5500 V, temperature 25 °C, ion source gas 1 (GS1) 45 $L \cdot min^{-1}$; ion source gas 2 (GS2) 0 $L \cdot min^{-1}$; curtain gas (CUR) 12 $L \cdot min^{-1}$, declustering potential (DP) 150 V, collision energy (CE) 10 V, acquisition range 1000–2600 *m/z*; for Cyt c, HEWL and Ub positive polarity, ionspray voltage floating 5500 V, temperature 25 °C, ion source gas 1 (GS1) 35 $L \cdot min^{-1}$; ion source gas 2 (GS2) 0 $L \cdot min^{-1}$; curtain gas (CUR) 20 $L \cdot min^{-1}$, declustering potential (DP) 180 V, collision energy (CE) 10 V, acquisition range 500–1800 *m/z*; for SOD positive polarity, ionspray voltage floating 5500 V, temperature 25 °C, ion source gas 1 (GS1) 40 $L \cdot min^{-1}$; ion source gas 2 (GS2) 0 $L \cdot min^{-1}$; curtain gas (CUR) 15 $L \cdot min^{-1}$, declustering potential (DP) 200 V, collision energy (CE) 10 V, acquisition range 1500–3500 *m/z*; for CA I positive polarity, ionspray voltage floating 5500 V, temperature 25 °C, ion source gas 1 (GS1) 50 $L \cdot min^{-1}$; ion source gas 2 (GS2) 0 $L \cdot min^{-1}$; curtain gas (CUR) 20 $L \cdot min^{-1}$, declustering potential (DP) 50 V, collision energy (CE) 10 V, acquisition range

600–1400 *m/z*, for ODN2 negative polarity, ionspray voltage floating -4500 V, temperature 25 °C, ion source gas 1 (GS1) 35 $L \cdot min^{-1}$; ion source gas 2 (GS2) 0 $L \cdot min^{-1}$; curtain gas (CUR) 25 $L \cdot min^{-1}$, declustering potential (DP) -30 V, collision energy (CE) -10 V, acquisition range 500–2000 *m/z*. For the spectra recording, Analyst TF software 1.7.1 (Sciex, Framingham, MA, USA) was used and deconvoluted spectra were obtained by using the Bio Tool Kit micro-application v.2.2 embedded in PeakView™ software v.2.2 (Sciex, Framingham, MA, USA).

Acknowledgements

We gratefully thank the University of Pisa for financial support (PRA_2020_39). AP thanks Prof. Luigi Messori (Dept. of Chemistry "U. Schiff", University of Florence) for making available the TripleTOF® 5600+ mass spectrometer (Sciex, Framingham, MA, U.S.A.).

Supporting Information Available

IR and NMR spectra of products; NMR data for complexes in CD_3OD/D_2O solutions; spectroelectrochemical studies; ROS analyses (3 hours); HR-ESI-MS spectra of products and isotopic pattern simulations; HR-ESI-MS studies on the interaction of complexes with biomolecules. CCDC reference numbers 2073921 (**[2a]CF_3SO_3**) and 2073922 (**3**) contain the supplementary crystallographic data for the single crystal X-ray studies reported in this paper. These data can be obtained free of charge at www.ccdc.cam.ac.uk/conts/retrieving.html (or from the Cambridge Crystallographic Data Centre, 12, Union Road, Cambridge CB2 1EZ, UK; fax: (internat.) +44-1223/336-033; e-mail: deposit@ccdc.cam.ac.uk).

References

1 H. Sung, J. Ferlay, R. L. Siegel, M. Laversanne, I. Soerjomataram, A. Jemal and F. Bray, Global cancer statistics 2020: GLOBOCAN estimates of incidence and mortality worldwide for 36 cancers in 185 countries. *CA: A Cancer Journal for Clinicians*, 2021, **71**, 209-249.

2 (a) I. A. Riddell and S. J. Lippard, Cisplatin and Oxaliplatin: Our Current Understanding of Their Actions. *Met. Ions Life Sci*. 2018, **18**, 1–42. (b) M. G. Apps, E. H. Y. Choi and N. J. Wheate, The state-of-play and future of platinum drugs. *Endocrine-Related Cancer* 2015, **22**, R219–R233. (c) C. Yu, Z. Wang, Z. Sun, L. Zhang, W. Zhang, Y. Xu and J.-J. Zhang, *Platinum-Based Combination Therapy: Molecular Rationale, Current Clinical Uses, and Future Perspectives*. *J. Med. Chem*. 2020, **63**, 13397-13412.

3 (a) R. Oun, Y. E. Moussa and N. J. Wheate, The side effects of platinum-based chemotherapy drugs: a review for chemists. *Dalton Trans.* 2018, **47**, 6645-6653. (b) Z. H. Siddik, Cisplatin: mode of cytotoxic action and molecular basis of resistance. *Oncogene* 2003, **22**, 7265-7279.

4 D. Gibson, Platinum(IV) anticancer agents; are we en route to the holy grail or to a dead end? *J. Inorg. Biochem*. 2021, **217**, 111353.

5 (a) B. S. Murray and P. J. Dyson, Recent progress in the development of organometallics for the treatment of cancer. *Curr. Opinion Chem. Biol*., 2020, **56**, 28-34. (b) P. Štarha and Z. Trávníček, Non-platinum complexes containing releasable biologically active ligands. *Coord. Chem. Rev*., 2019, **395**, 130-145. (c) I. Bratsos, T. Gianferrara, E. Alessio, C. G. Hartinger, M. A. Jakupec and B. K. Keppler. *Ruthenium and Other Non-Platinum Anticancer Compounds, in Bioinorganic Medicinal Chemistry*, ed. E. Alessio, Wiley-VCH, Weinheim, 2011, 151-174. (d) A. L. Noffke, A. Habtemariam, A. M. Pizarro and P. J. Sadler, Designing organometallic compounds for catalysis and therapy. *Chem. Commun*., 2012, **48**, 5219-5246. (e) Y. C. Ong and G. Gasser, Organometallic compounds in drug discovery: Past, present and future. *Drug Discovery Today* 2020, **37**, 117-124.

6 (a) E. Boros, P. J. Dyson and G. Gasser, Classification of Metal-Based Drugs according to Their Mechanisms of Action. *Chem* 2020, **6**, 41–60. (b) E. J. Anthony, E. M. Bolitho, H. E. Bridgewater, O. W. L. Carter, J. M. Donnelly, C. Imberti, E. C. Lant, F. Lermyte, R.J. Needham, M. Palau, P. J. Sadler, H. Shi, F.-X. Wang, W.-Y. Zhang and Z. Zhang, Metallodrugs are unique: opportunities and challenges of discovery and development. *Chem. Sci*. 2020, **11**, 12888-12917. (b) K. L. Haas and K. J. Franz. Application of Metal Coordination Chemistry To Explore and Manipulate Cell Biology. *Chem. Rev*. 2009, **109**, 4921–4960. (c) G. Gasser and N. Metzler-Nolte, The potential of organometallic complexes in medicinal chemistry. *Curr. Opinion Chem. Biol*. 2012, **16**, 84–91.

7 (a) U. Basu, M. Roy and A. R. Chakravarty, Recent advances in the chemistry of iron-based chemotherapeutic agents. *Coord. Chem. Rev*. 2020, **417**, 213339. (b) A. A. Simenel, E. A. Morozova, L. V.

Snegur, S. I. Zykova, V. V. Kachala, L. A. Ostrovskaya, N. V. Bluchterova and M. M. Fomina, *Appl. Organometal. Chem*. 2009, **23**, 219–224.

8 (a) M. Patra and G. Gasser, The medicinal chemistry of ferrocene and its derivatives. *Nat. Chem. Rev*. 2017, **1**, 66. (b) S. Sansook, S. Hassell-Hart, C. Ocasio and J. Spencer, Ferrocenes in medicinal chemistry; a personal perspective. *J. Organomet. Chem*. 2020, **905**, 121017.

9 Y. Wang, P. M. Dansette, P. Pigeon, S. Top, M. J. McGlinchey, D. Mansuy and G. Jaouen, A new generation of ferrociphenols leads to a great diversity of reactive metabolites, and exhibits remarkable antiproliferative properties. *Chem. Sci.*, 2018, **9**, 70–78.

10 (a) O. Buriez, J. M. Heldt, E. Labb, A. Vessières, G. Jaouen and C. Amatore, Reactivity and Antiproliferative Activity of Ferrocenyl–Tamoxifen Adducts with Cyclodextrins against Hormone-Independent Breast-Cancer Cell Lines. *Chem. Eur. J*., 2008, **14**, 8195-8203. (b) A. Vessières, Y. Wang, M. J. McGlinchey and G. Jaouen, Multifaceted chemical behaviour of metallocene (M = Fe, Os) quinone methides. Their contribution to biology. *Coord. Chem. Rev*. 2021, **430**, 213658. (c) P. Idlas, E. Lepeltier, G. Jaouen and C. Passirani, Ferrocifen Loaded Lipid Nanocapsules: A Promising Anticancer Medication against Multidrug Resistant Tumors. *Cancers* 2021, **13**, 2291.

11 Selected recent reviews: (a) A. Singh, I. Lumb, V. Mehra and V. Kumar, Ferrocene-appended pharmacophores: an exciting approach for modulating the biological potential of organic scaffolds. *Dalton Trans*. 2019, **48**, 2840-2860. (b) R. Wang, H. Chen, W. Yan, M. Zheng, T. Zhang and Y. Zhang, Ferrocene-containing hybrids as potential anticancer agents: Current developments, mechanisms of action and structure-activity relationships. *Eur. J. Med. Chem*. 2020, **190**, 112109. (c) B. Sharma and V. Kumar, Has Ferrocene Really Delivered Its Role in Accentuating the Bioactivity of Organic Scaffolds. *J. Med. Chem*. 2021, **64**, 16865-16921.

12 Relevant publications include: (a) M. K. Ismail, Z. Khan, M. Rana, S. L. Horswell, L. Male, H. V. Nguyen, A. Perotti, I. Romero-Canelon, E. A. Wilkinson, N. J. Hodges and J. H. R. Tucker. Effect of Regiochemistry and Methylation on the Anticancer Activity of a Ferrocene-Containing Organometallic Nucleoside Analogue. *ChemBioChem* 2020, **21**, 2487-2494. (b) L. Zeng, M. Tang, C. Pi, J. Zheng, S. Gao, T. Chabanne, R. Chauvin, W. Cheng, H. Lin, R. Xu and C. Cui. Novel Ferrocene Derivatives Induce Apoptosis through Mitochondria-Dependent and Cell Cycle Arrest via PI3K/Akt/mTOR Signaling Pathway in T Cell Acute Lymphoblastic Leukemia. *Cancers,* 2021, **13**, 4677. (c) A. Wieczorek-Blauz, K. Kowalczyk, A. Blauz, A. Makal, S. Pawledzio, C. Eurtivong, H. J. Arabshahi, J. Reynisson, C. G. Hartinger, B. Rychlik and D. Plazuk. Impact of the ferrocenyl group on cytotoxicity and KSP inhibitory activity of ferrocenyl monastrol conjugates. *Dalton Trans*., 2022, **51**, 491-508. (d) A. A. Simenel, E. A.

Morozova, L. V. Snegur, S. I. Zykova, V. V. Kachala, L. A. Ostrovskaya, N. V. Bluchterova and M. M. Fomina, Simple route to ferrocenylalkyl nucleobases. Antitumor activity in vivo. *Appl. Organometal. Chem*., 2009, **23**, 219–224.

13 Selected recent references: (a) W. Villarreal, L. Colina-Vegas, C. Rodrigues de Oliveira, J. C. Tenorio, J. Ellena, F. C. Gozzo, M. R. Cominetti, A. G. Ferreira, M. A. B. Ferreira, M. Navarro and A. A. Batista. Chiral Platinum(II) Complexes Featuring Phosphine and Chloroquine Ligands as Cytotoxic and Monofunctional DNA-Binding Agents. *Inorg. Chem*. 2015, **54**, 11709-11720. (b) J. Banfic, A. A. Legin, M. A. Jakupec, M. Galanski and B. K. Keppler. Platinum(IV) Complexes Featuring One or Two Axial Ferrocene Bearing Ligands - Synthesis, Characterization, and Cytotoxicity. *Eur. J. Inorg. Chem*. 2014, 484-492. (c) F. Rivas, A. Medeiros, M. Comini, L. Suescun, E. Rodriguez Arce, M. Martins, T. Pinheiro, F. Marques and D. Gambino. Pt-Fe ferrocenyl compounds with hydroxyquinoline ligands show selective cytotoxicity on highly proliferative cells. *J. Inorg. Biochem*. 2019, **199**, 110779.

14 Selected recent references: (a) C. M. Anderson, S. S. Jain, L. Silber, K. Chen, S. Guha, W. Zhang, E. C. McLaughlin, Y. Hu and J. M. Tanski, Synthesis and characterization of water-soluble, heteronuclear ruthenium(III)/ferrocene complexes and their interactions with biomolecules. *J. Inorg. Biochem*. 2015, **145** (2015) 41–50. (b) C. Mu, K. E. Prosser, S. Harrypersad, G. A. MacNeil, R. Panchmatia, J. R. Thompson, S. Sinha, J. J. Warren and C. J. Walsby, Activation by Oxidation: Ferrocene-Functionalized Ru(II)-Arene Complexes with Anticancer, Antibacterial, and Antioxidant Properties. *Inorg. Chem*. 2018, **57**, 15247−15261. (c) D. Gelle, M. Lamac, K. Mach, L. Simkova, R. Gyepes, L. Sommerova, A. Martisova, M. Bartosik, T. Vaculovic, V. Kanicky, R. Hrstka and J. Pinkas. Enhanced Intracellular Accumulation and Cytotoxicity of Ferrocene-Ruthenium Arene Conjugates. *ChemPlusChem* 2020, **85**, 1034-1043.

15 (a) L. Tabrizi and H. Chiniforoshan. The cytotoxicity and mechanism of action of new multinuclear Scaffold Au^{III}, Pd^{II} pincer complexes containing a bis(diphenylphosphino) ferrocene/non-ferrocene ligand. *Dalton Trans*. 2017, **46**, 14164-14173. (b) G. Gong, Y. Cao, F. Wang and G. Zhao, Planar Chiral Ferrocene Cyclopalladated Derivatives Induce Caspase- Dependent Apoptosis and Antimetastasis in Cancer Cells. *Organometallics* 2018, **37**, 1103−1113.

16 H. Zeh, P. Haines, M. E. Miehlich, T. Kienz, A. Neidlinger, R. P. Friedrich, H. G. Özkan, C. Alexiou, F. Hampel, D. M. Guldi, K. Meyer, J. Schatz, K. Heinze and A. Mokhir. Anticancer Effect of an Electronically Coupled Oligoferrocene. *Organometallics* 2020, **39**, 3112-3120.

17 (a) A. Pilon, A. R. Brás, L. Côrte-Real, F. Avecilla, P. J. Costa, A. Preto, M. H. Garcia and A. Valente. A New Family of Iron(II)-Cyclopentadienyl Compounds Shows Strong Activity against Colorectal and Triple Negative Breast Cancer Cells. *Molecules* 2020, **25**, 1592, and references therein. (b) H. T. Poh and P. C. Ho, W. Y. Fan. Cyclopentadienyl iron dicarbonyl ($CpFe(CO)_2$) derivatives as apoptosis-inducing agents.

RSC Adv., 2016, **6**, 18814–18823. (c) P. R. Florindo, D. M. Pereira, P. M. Borralho, C. M. P. Rodrigues, M. F. M. Piedade and A. C. Fernandes. Cyclopentadienyl − Ruthenium(II) and Iron(II) Organometallic Compounds with Carbohydrate Derivative Ligands as Good Colorectal Anticancer Agents. *J. Med. Chem*. 2015, **58**, 4339 − 4347.

18 (a) X. Jiang, L. Chen, X. Wang, L. Long, Z. Xiao and X. Liu. Photoinduced Carbon Monoxide Release from Half-Sandwich Iron(II) Carbonyl Complexes by Visible Irradiation: Kinetic Analysis and Mechanistic Investigation. *Chem. Eur. J.* 2015, **21**, 13065-13072. (b) C. Johnson and M. Albrecht, Piano-stool N-heterocyclic carbene iron complexes: Synthesis, reactivity and catalytic applications. *Coord. Chem. Rev*., 2017, **352**, 1–14.

19 G. Agonigi, L. Biancalana, M. G. Lupo, M. Montopoli, N. Ferri, S. Zacchini, F. Binacchi, T. Biver, B. Campanella, G. Pampaloni, V. Zanotti and F. Marchetti, Exploring the Anticancer Potential of Diiron Bis-cyclopentadienyl Complexes with Bridging Hydrocarbyl Ligands: Behavior in Aqueous Media and In Vitro Cytotoxicity. *Organometallics* 2020, **39**, 645-657.

20 (a) V. Ritleng and M. J. Chetcuti, Hydrocarbyl Ligand Transformations on Heterobimetallic Complexes. *Chem. Rev*., 2007, **107**, 797−858. (b) G. Li, D. Zhu, X. Wang, Z. Su, M. R. Bryce, M. R. Dinuclear metal complexes: multifunctional properties and applications. *Chem. Soc. Rev*., 2020, **49**, 765-838. (c) B. S. Natinsky and C. Liu. Two are better than one. *Nat. Chem*., 2019, **11**, 199–203.

21 (a) L. R. Almazahreh, F. Arrigoni, H. Abul-Futouh, M. El-khateeb, H. Goerls, C. Elleouet, P. Schollhammer, L. Bertini, L. De Gioia, M. Rudolph, G. Zampella and W. Weigand. Proton Shuttle Mediated by $(SCH_2)_2P{=}O$ Moiety in [FeFe]-Hydrogenase Mimics: Electrochemical and DFT Studies. *ACS Catal*., 2021, **11**, 7080-7098 (b) H. Land, M. Senger, G. Berggren and S. Stripp, Current State of [FeFe]-Hydrogenase Research: Biodiversity and Spectroscopic Investigations. *ACS Catal*., 2020, **10**, 7069-7086.

22 (a) R. Mazzoni, M. Salmi and V. Zanotti, C-C Bond Formation in Diiron Complexes. *Chem. Eur. J*., 2012, **18**, 10174-10194. (b) L. Biancalana and F. Marchetti, Aminocarbyne ligands in organometallic chemistry. *Coord. Chem. Rev*., 2021, **449**, 214203.

23 L. Biancalana, M. De Franco, G. Ciancaleoni, S. Zacchini, G. Pampaloni, V. Gandin and F. Marchetti, Easily Available and Amphiphilic Diiron Cyclopentadienyl Complexes Exhibit In Vitro Anticancer Activity in 2D and 3D Human Cancer Cells via Redox Modulation Triggered by CO Release. *Chem. Eur. J*., 2021, **27**, 10169–10185.

24 (a) D. Rocco, L. K. Batchelor, G. Agonigi, S. Braccini, F. Chiellini, S. Schoch, T. Biver, T. Funaioli, S. Zacchini, L. Biancalana, M. Ruggeri, G. Pampaloni, P. J. Dyson and F. Marchetti, Anticancer Potential of Diiron Vinyliminium Complexes. *Chem. Eur. J*., 2019, **25**, 14801-14816. (b) G. Agonigi, L. K. Batchelor, E. Ferretti, S. Schoch, M. Bortoluzzi, S. Braccini, F. Chiellini, L. Biancalana, S. Zacchini, G. Pampaloni, B.

Sarkar, P. J. Dyson and F. Marchetti, Mono-, Di- and Tetra-iron Complexes with Selenium or Sulphur Functionalized Vinyliminium Ligands: Synthesis, Structural Characterization and Antiproliferative Activity. *Molecules*, 2020, **25**, 1656.

25 S. Braccini, G. Rizzi, L. Biancalana, A. Pratesi, S. Zacchini, G. Pampaloni, F. Chiellini and F. Marchetti, Anticancer Diiron Vinyliminium Complexes: A Structure–Activity Relationship Study. *Pharmaceutics,* 2021, **13**, 1158.

26 (a) S. Schoch, M. Hadiji, S. A. P. Pereira, M. L. M. F. S. Saraiva, S. Braccini, F. Chiellini, T. Biver, S. Zacchini, G. Pampaloni, P. J. Dyson and F. Marchetti, A Strategy to Conjugate Bioactive Fragments to Cytotoxic Diiron Bis-Cyclopentadienyl Complexes. *Organometallics,* 2021, **40**, 2516 − 2528. (b) S. Schoch, D. Iacopini, M. Dalla Pozza, S. Di Pietro, I. Degano, G. Gasser, V. Di Bussolo and F. Marchetti, Tethering Carbohydrates to the Vinyliminium Ligand of Antiproliferative Organometallic Diiron Complexes. *Organometallics,* 2022, **41**, 514–526.

27 G. Agonigi, M. Bortoluzzi, F. Marchetti, G. Pampaloni, S. Zacchini and V. Zanotti. Additions to Diiron Carbonyl Complexes Containing a Bridging Aminocarbyne Ligand: A Synthetic, Crystallographic and DFT Study. *Eur. J. Inorg. Chem*., 2018, 960–971.

28 (a) V. G. Albano, L. Busetto, M. Monari and V. Zanotti, Reactions of acetonitrile di-iron μ-aminocarbyne complexes; synthesis and structure of $[Fe_2(\mu\text{-}CNMe_2)(\mu\text{-}H)(CO)_2(Cp)_2]$. *J. Organomet. Chem*., 2000, **606**, 163–168. (b) V. G. Albano, L. Busetto, F. Marchetti, M. Monari, S. Zacchini and V. Zanotti, Diiron í-Vinyliminium Complexes from Acetylene Insertion into a Metal - Aminocarbyne Bond. *Organometallics,* 2003, **22**, 1326-1331.

29 L. Busetto, R. Mazzoni, M. Salmi, S. Zacchini and V. Zanotti, Ethynylferrocene insertion into Fe-C bond in bridging aminocarbyne diiron complexes: New triiron vinyliminium complexes. *J. Organomet. Chem*., 2010, **695**, 2519-2525.

30 L. Biancalana, M. Kubeil, S. Schoch, S. Zacchini, F. Marchetti, Switching on Cytotoxicity of Water-Soluble Diiron Organometallics by UV Irradiation, *Inorg. Chem.* 2022, **61**, 7897–7909.

31 G. Agonigi, M. Bortoluzzi, F. Marchetti, G. Pampaloni, S. Zacchini and V. Zanotti. Additions to Diiron Carbonyl Complexes Containing a Bridging Aminocarbyne Ligand: A Synthetic, Crystallographic and DFT Study. *Eur. J. Inorg. Chem*., 2018, 960–971.

32 F. Marchetti. Constructing Organometallic Architectures from Aminoalkylidyne Diiron Complexes. *Eur. J. Inorg. Chem*., 2018, 3987–4003

33 S. Schoch, L. K. Batchelor, T. Funaioli, G. Ciancaleoni, S. Zacchini, S. Braccini, F. Chiellini, T. Biver, G. Pampaloni, P. J. Dyson and F. Marchetti, Diiron Complexes with a Bridging Functionalized Allylidene Ligand: Synthesis, Structural Aspects, and Cytotoxicity. *Organometallics,* 2020, **39**, 361-373.

34 M. Marloye, G. Berger, M. Gelbcke and F. Dufrasne, A survey of the mechanisms of action of anticancer transition metal complexes. *Fut. Med. Chem*. 2016, **8**, 2263-2286.

35 Methanol was used as a co-solvent to obtain mM solutions of the compounds as required by the technique used (^{1}H NMR).

36 (a) X. Jiang, Z. Xiao, W. Zhong and X. Liu, Brief survey of diiron and monoiron carbonyl complexes and their potentials as CO-releasing molecules (CORMs). *Coord. Chem. Rev*., 2021, **429**, 213634. (b) T. Thuy, T. Vo, Q. Canh Vo, V. P. Tuan, Y. Wee, H.-C. Cheng, I-T. Lee, The potentials of carbon monoxide-releasing molecules in cancer treatment: An outlook from ROS biology and medicine. *Redox Biology* 2021, **46**, 102124.

37 G. Provinciali, M. Bortoluzzi, T. Funaioli, S. Zacchini, B. Campanella, G. Pampaloni and F. Marchetti, Tetrasubstituted Selenophenes from the Stepwise Assembly of Molecular Fragments on a Diiron Frame and Final Cleavage of a Bridging Alkylidene. *Inorg. Chem*., 2020, **59**, 17497-17508.

38 (a) E. Reisner, V. B. Arion, M.F.C. Guedes da Silva, R. Lichtenecker, A. Eichinger, B. K. Keppler, V. Yu. Kukushkin, A. J. L. Pombeiro, Tuning of Redox Potentials for the Design of Ruthenium Anticancer Drugs - an Electrochemical Study of [trans-$RuCl_4L(DMSO)$]- and [trans-$RuCl_4L_2$]$^-$ Complexes, where L = Imidazole, 1,2,4-Triazole, Indazole. *Inorg. Chem*., 2004, **43**, 7083-7093. (b) W.G. Kirlin, J. Cai, S.A. Thompson and D. Diaz, Glutathione Redox Potential in Response to Differentiation and Enzyme Inducers. *Free Radical Biology & Medicine,* 1999, **27**, 1208-1218.

39 (a) D. Miklavcic, G. Sersa and S. Novakovic, Tumor Bioelectric Potential and its Possible Exploitation for Tumor Growth Retardation. *J. Bioelect*., 1990, **9**, 133-149. (b) M. J. Clarke, Ruthenium Metallapharmaceuticals. *Coord. Chem. Rev*., 2003, **236**, 209-233.

40 V. Raičević, N. Radulović., L. Jovanović, M. Rodić, I. Kuzminac, D. Jakimov, T. Wrodnigg, T.O. Knedel, C. Janiak and M. Sakač, Ferrocenylmethylation of estrone and estradiol: Structure, electrochemistry, and antiproliferative activity of new ferrocene–steroid conjugates. *Appl. Organomet. Chem*., 2020, **34**, e5889.

41 S. Realista, S. Quintal, P. N. Martinho, A.I. Melato, A. Gil, T. Esteves, M. De Deus Carvalho, L. P. Ferreira, P. D. Vaz and M. J. Calhorda, Electrochemical studies and potential anticancer activity in ferrocene derivatives. *J. Coord. Chem*., 2017, **70**, 314-327.

42 (a) A. Leonidova, P. Anstaett, V. Pierroz, C. Mari, B. Spingler, S. Ferrari and G. Gasser, Induction of Cytotoxicity through Photorelease of Aminoferrocene. *Inorg. Chem*., 2015, **54**, 9740−9748. (b) P. Marzenell, H. Hagen, L. Sellner, T. Zenz, R. Grinyte, V. Pavlov, S. Daum and A. Mokhir, Aminoferrocene-

Based Prodrugs and Their Effects on Human Normal and Cancer Cells as Well as Bacterial Cells. *J. Med. Chem.*, 2013, **56**, 6935-6944.

43 (a) L. Messori and A. Merlino. Protein metalation by metal-based drugs: X-ray crystallography and mass spectrometry studies. *Chem. Commun*., 2017, **53**, 11622-11633, (b) A. Casini, G. Mastrobuoni, M. Terenghi, C. Gabbiani, E. Monzani, G. Moneti, L. Casella and L. Messori, Ruthenium anticancer drugs and proteins: a study of the interactions of the ruthenium(III) complex imidazolium trans-[tetrachloro(dimethyl sulfoxide)(imidazole)ruthenate(III)] with hen egg white lysozyme and horse heart cytochrome c. *J. Biol. Inorg. Chem*. 2007, **12**, 1107-1117. (c) A. Merlino, Recent advances in protein metalation: structural studies. *Chem. Commun*., 2021, **57**, 1295-1307.

44 A. Pratesi, D. Cirri, L. Ciofi and L. Messori, Reactions of Auranofin and Its Pseudohalide Derivatives with Serum Albumin Investigated through ESI-Q-TOF MS. *Inorg. Chem*., 2018, **57**, 10507-10510.

45 R. Ye, C. Tan, B. Chen, R. Li and Z. Mao, Zinc-Containing Metalloenzymes: Inhibition by Metal-Based Anticancer Agents. *Front. Chem*., 2020, **8**, 402.

46 Selected recent reviews: (a) J. Zhang, X. Li, X. Han, R. Liu and J. Fang, Targeting the Thioredoxin System for Cancer Therapy. *Trends Pharmacol. Sci*., 2017, **38**, 794-808. (b) J. Lu, E.-H. Chew and A. Holmgren, Targeting thioredoxin reductase is a basis for cancer therapy by arsenic trioxide. *Proc. Natl. Acad. Sci. USA*, 2007, **104**, 12288-12293. (c) A. Bindoli, M. P. Rigobello, G. Scutari, C. Gabbiani, A. Casini and L. Messori, Thioredoxin reductase: A target for gold compounds acting as potential anticancer drugs. *Coord. Chem. Rev*., 2009, **253**, 1692-1707. (d) M. Bian, R. Fan, S. Zhao and W. Liu, Targeting the Thioredoxin System as a Strategy for Cancer Therapy. *J. Med. Chem*., 2019, **62**, 7309-7321.

47 (a) V. Scalcon, M. Salmain, A. Folda, S. Top, P. Pigeon, H. Z. Shirley Lee, G. Jaouen, A. Bindoli, A. Vessiéres and M. P. Rigobello, Tamoxifen-like metallocifens target the thioredoxin system determining mitochondrial impairment leading to apoptosis in Jurkat cells. *Metallomics*, 2017, **9**, 949--959. (b) L. Xie, Z. Luo, Z. Zhao and T. Chen, Anticancer and Antiangiogenic Iron(II) Complexes That Target Thioredoxin Reductase to Trigger Cancer Cell Apoptosis. *J. Med. Chem*., 2017, **60**, 202−214. (c) V. Scalcon, A. Citta, A. Folda, A. Bindoli, M. Salmain, I. Ciofini, S. Blanchard, J. de Jésús Cázares-Marinero, Y. Wang, P. Pigeon, G. Jaouen, A. Vessières and M. P. Rigobello, Enzymatic oxidation of ansa-ferrocifen leads to strong and selective thioredoxin reductase inhibition in vitro. *J. Inorg. Biochem*., 2016, **165**, 146–151.

48 Human pancreatic PSN-1 cells treated with 25μM of [**1b**]CF_3SO_3 and [**1e**]CF_3SO_3 for 24 hours showed a residual TrxR cellular activity of 57% and 39%, respectively. TrxR activity was tested by measuring NADPH dependent reduction of DTNB.

49 A. Pratesi, C. Gabbiani, E. Michelucci, M. Ginanneschi, A. M. Papini, R. Rubbiani, I. Ott and L. Messori, Insights on the mechanism of thioredoxin reductase inhibition by gold N-heterocyclic carbene compounds

using the synthetic linear selenocysteine containing C-terminal peptide hTrxR(488-499): An ESI-MS investigation. *J. Inorg. Biochem*., 2014, **136**, 161–169.

50 C. Mügge, D. Musumeci, E. Michelucci, F. Porru, T. Marzo, L. Massai, L. Messori, W. Weigand and D. Montesarchio. Elucidating the reactivity of Pt(II) complexes with (O,S) bidentate ligands towards DNA model systems. *J. Inorg. Biochem*., 2016, **160**, 198-209.

51 F. Menges, "Spectragryph - optical spectroscopy software", Version 1.2.5, @ 2016-2017, http://www.effemm2.de/spectragryph.

52 G. R. Fulmer, A. J. M. Miller, N. H. Sherden, H. E. Gottlieb, A. Nudelman, B. M. Stoltz, J. E. Bercaw and K. I. Goldberg. NMR Chemical Shifts of Trace Impurities: Common Laboratory Solvents, Organics, and Gases in Deuterated Solvents Relevant to the Organometallic Chemist. *Organometallics,* 2010, **29**, 2176–2179.

53 R. K. Harris, E. D. Becker, S. M. Cabral De Menezes, R. Goodfellow and P. Granger, NMR nomenclature. Nuclear spin properties and conventions for chemical shifts(IUPAC Recommendations 2001). *Pure Appl. Chem*., 2001, **73**, 1795–1818.

54 W. Willker, D. Leibfritz, R. Kerssebaum and W. Bermel. Gradient selection in inverse heteronuclear correlation spectroscopy. *Magn. Reson. Chem*., 1993, **31**, 287-292.

55 G. M. Sheldrick, SADABS-2008/1 - Bruker AXS Area Detector Scaling and Absorption Correction, Bruker AXS: Madison, Wisconsin, USA, 2008.

56 G. M. Sheldrick, Crystal structure refinement with SHELXL. *Acta Crystallogr. C*, 2015, **71**, 3.

57 Calculated by the formula pD = pH* + 0.4, where pH* is the value measured for H_2O-calibrated pH-meter. a) C. C. Westcott, pH Measurements; Academic Press: New York, 1978. b) A. K. Covington, M. Paabo, R. A. Robinson and R. G. Bates, *Anal. Chem*. 1968, **40**, 700-706.

58 L. Biancalana, L. K. Batchelor, T. Funaioli, S. Zacchini, M. Bortoluzzi, G. Pampaloni, P. J. Dyson and F. Marchetti, α-Diimines as Versatile, Derivatizable Ligands in Ruthenium(II) p-Cymene Anticancer Complexes. *Inorg. Chem*., 2018, **57**, 6669 − 6685.

59 M. Krejčik, M. Daněk and F. Hartl. Simple construction of an infrared optically transparent thin-layer electrochemical cell: Applications to the redox reactions of ferrocene, $Mn_2(CO)_{10}$ and $Mn(CO)_3$(3,5-di-t-butyl-catecholate). *J. Electroanal. Chem*., 1991, **317**, 179-187.

60 G. Canil, S. Braccini, T. Marzo, L. Marchetti, A. Pratesi, T. Biver, T. Funaioli, F. Chiellini, J. D. Hoeschele and C. Gabbiani, *Dalton Trans*., 2019, ***48***, 10933-10944.

61 S. Ciambellotti, A. Pratesi, M. Severi, G. Ferraro, E. Alessio, A. Merlino and L. Messori, *Dalton Trans*., 2018, **47**, 11429-11437.

62 A. Rogue, C. Lambert, R. Josse, S. Antherieu, C. Spire, N. Claude, A. Guillouzo, Comparative Gene Expression Profiles Induced by PPARχ and PPARα/γ Agonists in Human Hepatocytes, *PLoS ONE* 2011, **6**, e18816.